Precambrian Research 383 (2022) 106909

Contents lists available at ScienceDirect

Precambrian Research

journal homepage: www.elsevier.com/locate/precamres

Paleomagnetism of the Ediacaran Avellaneda Formation (Argentina), part I: Paleogeography of the Río de la Plata craton at the dawn of Gondwana

P.R. Franceschinis [a,b,*], J.W. Afonso [c], M.J. Arrouy [d,b], L.E. Gómez-Peral [e,b], D. Poiré [e,b], R.I. F. Trindade [c], A.E. Rapalini [a,b]

[a] Universidad de Buenos Aires, Laboratorio de Paleomagnetismo Daniel A. Valencio, Instituto de Geociencias Básicas, Aplicadas y Ambientales de Buenos Aires (IGEBA), Departamento de Ciencias Geológicas, Facultad de Ciencias Exactas y Naturales, Buenos Aires, Argentina
[b] CONICET, Argentina
[c] Departamento de Geofísica, Instituto de Astronomia, Geofísica e Ciências Atmosféricas, Universidade de São Paulo, São Paulo, Brazil
[d] Instituto de Hidrología de Llanuras "Dr. E. J. Usunoff"- CONICET-, Argentina
[e] Centro de Investigaciones Geológicas, Facultad de Ciencias Naturales y Museo, La Plata, Argentina

ARTICLE INFO

Keywords:
Paleomagnetism
Avellaneda Formation
Cerro Negro Formation
Río de la Plata Craton
Ediacaran

ABSTRACT

A paleomagnetic and rock magnetic study was carried out in the Ediacaran Avellaneda (~570 Ma) and Cerro Negro (~555 Ma) Formations belonging to the La Providencia Group, in the upper part of the Neoproterozoic sedimentary cover of the Tandilia region, in the Río de la Plata craton. The Avellaneda Formation was studied at outcrop level and in three drill cores, yielding a mean characteristic remanence direction of Dec: 21.4°, Inc: 67.1°, α_{95}: 4.2°, k: 23.9, N: 51 and a paleomagnetic pole at 1.0° S, 313.4° E, A_{95}: 5.9°. The Cerro Negro Formation yielded a mean characteristic direction of Dec: 22.0°, Inc: 68.5°, α_{95}: 10.3°, k: 20.8, N: 11 obtained from a single drill core, from which a paleomagnetic pole at 3.6° S, 307.8°E, A_{95}: 16.6° was computed. Rock magnetic data indicates that magnetic remanence is mainly associated with magnetite and hematite. The paleomagnetic information presented here results in a change in the previously accepted Late Ediacaran apparent polar wander path of the Río de la Plata Craton. The newly obtained poles indicate that Río de la Plata Craton experienced a rapid drift from a low latitudes location (ca. 19° S) at ca. 600 Ma to moderately higher latitudes (between 50° and 42°S) from around 580 to 550 Ma.

1. Introduction

The Ediacaran period (635–539 Ma) witnessed a series of events of great importance such as the appearance and diversification of a complex biota (Erwin et al., 2011; Xiao et al., 2014, among others). At the same time, significant climatic changes occurred affecting the atmosphere composition and the chemistry of the oceans (eg. Canfield et al., 2008; Ader et al., 2009, 2014; Lyons et al., 2014; Sperling et al., 2015; Smith et al., 2016), which include a wide-spread glaciation (Gaskiers, Pu et al., 2016; Gómez-Peral et al., 2018; Poiré et al., 2018) and the largest negative excursion recorded in carbon isotopic composition (Shuram excursion, Macdonald et al., 2013; Gómez-Peral et al., 2018; Li et al., 2020). It has been speculated that all these processes have been directly related to global paleogeographic changes due to the final dispersal of the Rodinia supercontinent and the assembly of Gondwana (e.g. Collins and Pisarevsky, 2005; Li et al., 2013). In addition, the Ediacaran could have experienced very particular geomagnetic or geodynamic phenomena based on different non-actualist hypotheses. For example, geodynamic processes that led to episodes of inertial interchange true polar wander (IITPW) have been proposed (eg. Evans, 2003; Mitchell et al., 2012; Robert et al., 2017, 2018), or very peculiar geomagnetic patterns, such as the existence of a magnetic field with an equatorial dipole (Abrajevitch and Van der Voo, 2010) or a very weak geodynamo with permanent non-dipole configurations of the field (Driscoll, 2016). These hypotheses question the ability of the paleomagnetic method through the geocentric axial dipole (GAD) hypothesis to determine the paleolatitude and paleoorientation of the continents in the Ediacaran. These views may have been reinforced by recent absolute paleointensity determinations suggesting that during this period the Earth experienced an ultra-low geomagnetic field (e.g. Bono et al., 2019; Thallner et al.,

* Corresponding author at: Universidad de Buenos Aires, Laboratorio de Paleomagnetismo Daniel A. Valencio, Instituto de Geociencias Básicas, Aplicadas y Ambientales de Buenos Aires (IGEBA), Departamento de Ciencias Geológicas, Facultad de Ciencias Exactas y Naturales, Buenos Aires, Argentina.
E-mail address: pfrances@gl.fcen.uba.ar (P.R. Franceschinis).

https://doi.org/10.1016/j.precamres.2022.106909
Received 7 April 2022; Received in revised form 23 September 2022; Accepted 7 November 2022
Available online 18 November 2022

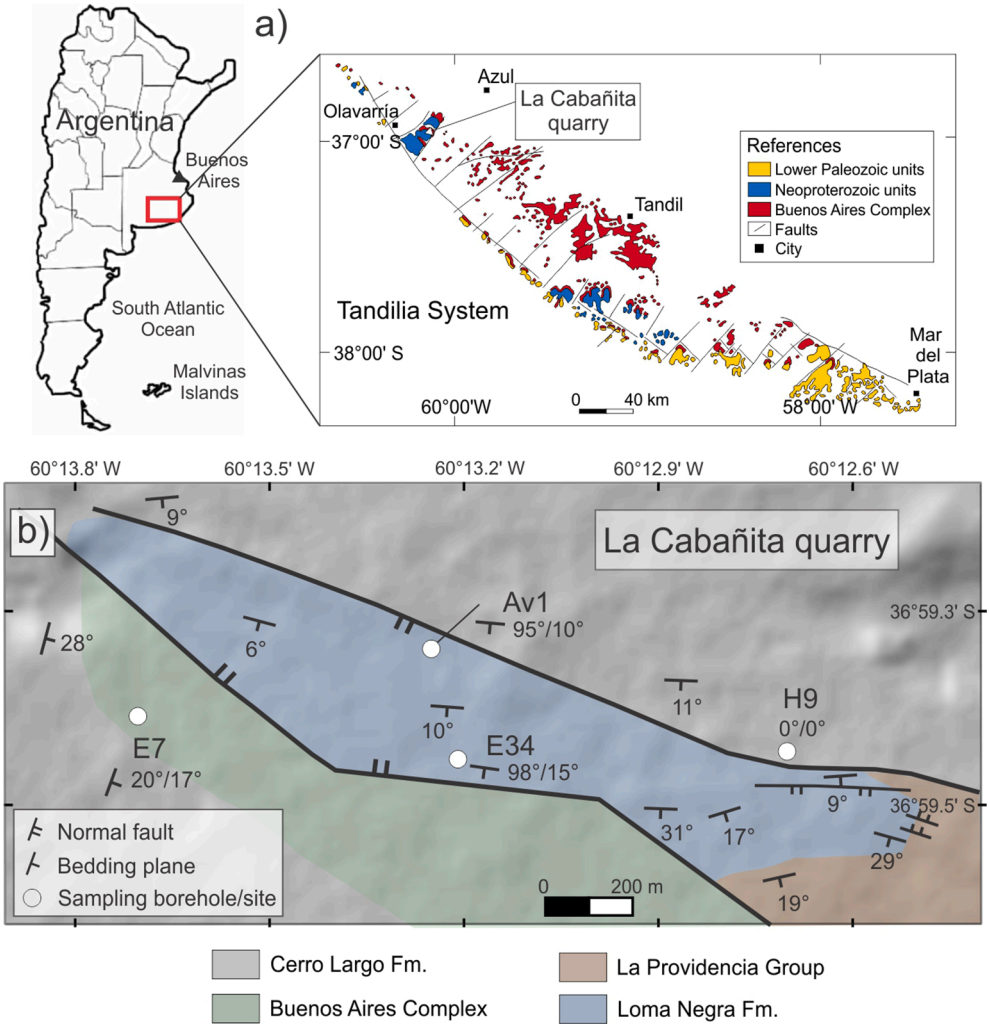

Fig. 1. A) Location of the study area, "La Cabañita" quarry in the Tandilia System, close to the Olavarría city; b) simplified geological map of the "La Cabañita" quarry where the location of the drill cores and the sampled site are indicated. modified map from Hernández et al. (2017). Note: the map published by Hernández et al. (2017) was carried out after the sampling of the AV1 site. The outcrops in the quarry changed due to the extraction works. In this way, the location of site AV1 currently corresponds to outcrops of the Loma Negra Formation. Bedding numbers: strike/dip (right hand convention).

2021). In contrast to those findings, some Ediacaran-Cambrian polar positions, with a high degree of reliability, have shown coherence along a relatively simple Gondwana apparent polar path, suggesting that the GAD hypothesis may still be valid for several intervals within, if not across most of the Ediacaran (for example, Tohver et al., 2006; Rapalini, 2018).

One of the major questions regarding the paleogeography of Western Gondwana from the Early Ediacaran to the Early Cambrian is the hypothesis, based on paleomagnetic data, of the existence of a large Clymene ocean between Amazonia-West Africa and Congo-São Francisco-Rio de La Plata (Trindade et al., 2006; Cordani et al., 2013; Tohver and Trindade, 2014; Rapalini et al., 2015). According to this hypothesis, the Amazon-West Africa block should have been the last major landmass to join Gondwana in the Early Cambrian. The existing paleomagnetic information in volcanic units of the middle Ediacaran of West Africa (Robert et al., 2017) allows a comparison of high quality contemporaneous paleomagnetic poles for the ~ 575 Ma of the Río de la Plata, West Africa and Congo-São Francisco cratons. The superposition of the poles of these cratons suggests that they were already united or very close to each other in the middle Ediacaran (Rapalini et al., 2021), weakening the model of a large Clymene ocean for those times (e.g. Rapalini et al., 2015). On the other hand, sedimentological and paleontological evidence has recently been interpreted as evidence for a still open Clymene Ocean in the late Ediacaran (Warren et al., 2014; Arrouy et al., 2016; Gómez-Peral et al., 2019; Arrouy and Gómez-Peral, 2021).

Paleomagnetic constraints on the paleogeographic evolution of the Río de la Plata craton (RPC) in the Precambrian is limited to three timespans (Rapalini et al., 2021). The first of them is restricted to the Rhyacian, between 2.11 and 2.05 Ga (Rapalini et al., 2015; Franceschinis et al., 2019). The second time span occurs during the Statherian and correspond to the 1790 Ma pole of Teixeira et al. (2013), which was obtained from the Florida tholeitic dyke swarm exposed in the Piedra Alta terrane, Uruguay. Finally, a third group of paleomagnetic poles and virtual geomagnetic poles (LB, Rapalini, 2006; SBd, SBe and SBf, Rapalini et al., 2013; SAn and PH, Rapalini et al., 2015) correspond to the Ediacaran, coeval with the assembly of Gondwana (600–550 Ma, Meert, 2014). The first paleomagnetic studies in Precambrian units of the Tandilia system, southern Río de la Plata craton, were carried out by Valencio et al. (1980) in sedimentary units assigned at that time to the La Tinta Formation (current Sierras Bayas Group). However, Rapalini and Sánchez Bettucci (2008) and Rapalini et al. (2013) demonstrated that these first studies had isolated a secondary remanence, likely related to a Permian to Triassic remagnetization. In the last twenty years, an apparent polar wander path (APWP) has been constructed with a total of six polar positions from paleomagnetic poles and VGPs for the Río de la Plata Craton (Rapalini et al., 2013; 2015; Rapalini, 2018). This path suggests that the craton was at low, nearly equatorial, latitudes at around 600 Ma and drifted to intermediate latitudes by 575 Ma, possibly already attached to or very close to the Congo-São Francisco and NW Africa cratons (Rapalini et al., 2021). By around 550 Ma, the RPC was still at intermediate latitudes. During the Ediacaran, besides this latitudinal migration, the RPC underwent a large counterclockwise

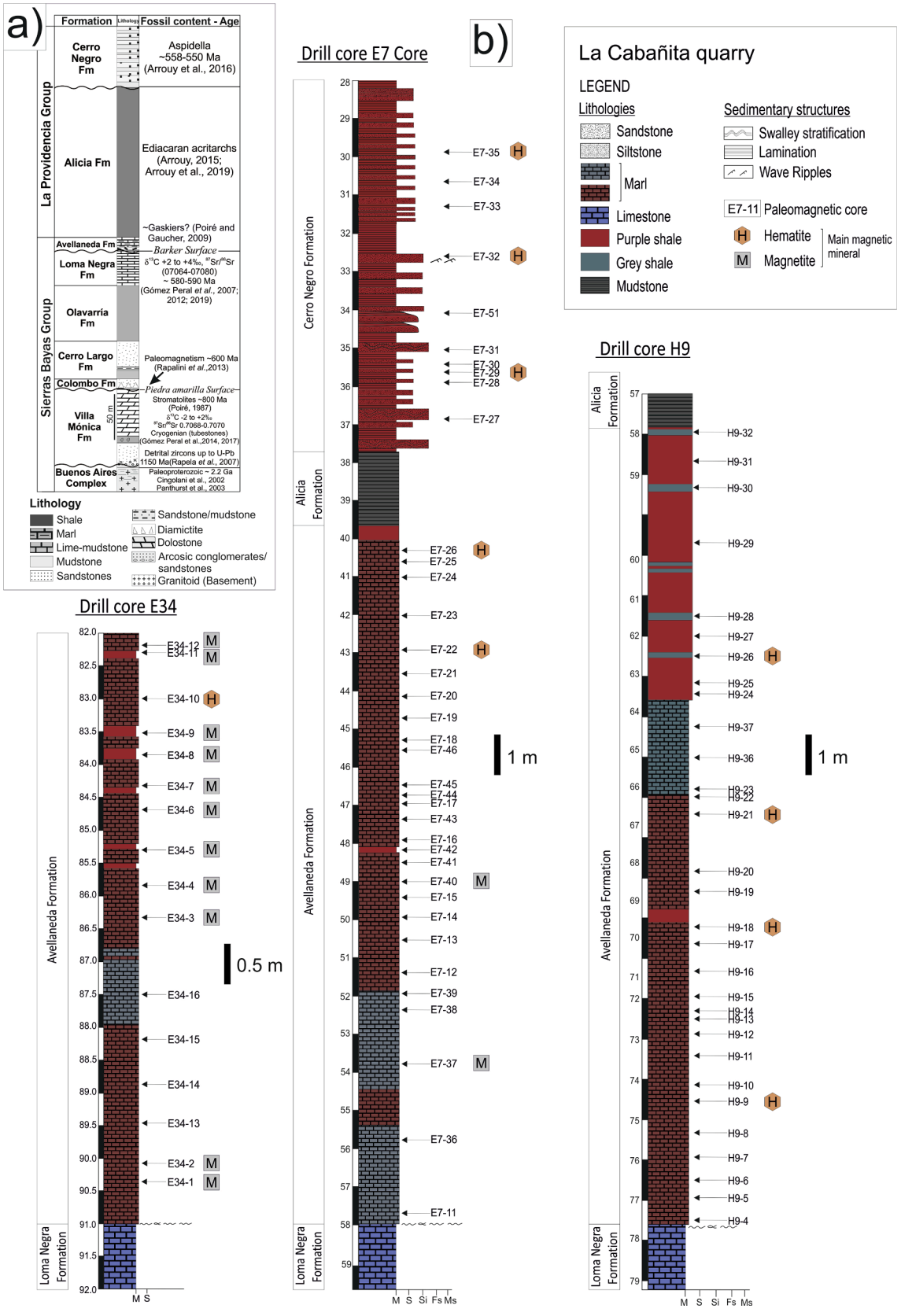

Fig. 2. A) Regional stratigraphic profile from Tandilia System. modified from Arrouy et al. (2019); b) Stratigraphic profiles of drill cores E34, E7 and H9. Stratigraphic position of each sample is indicated. The main magnetic mineral identified is indicated at different stratigraphic levels for each drill core. M: magnetite, H: hematite.

Fig. 3. A) and b) Quarry front where the Avellaneda Formation (site AV1) was sampled; c), d) and e) Samples extracted from the Avellaneda Formation in drill core E34. photos d) and e) belong to the same sample, showing the observed laminations in detail; f) and g) samples extracted from the Avellaneda Formation in drill core H9; h) and i) samples extracted from the Avellaneda Formation in drill core E7; j) drilled samples from the same formation with the individual cores; k) and l) samples extracted from the Cerro Negro Formation in drill core E7. note the fiduciary mark along the samples and the well-developed laminations, used for azimuthal orientation of the samples. See text for more information.

rotation. Lack of Neoproterozoic paleomagnetic data older than 600 Ma has prevented a paleomagnetic test of the position of this craton within Rodinia (e.g. Li et al., 2013). However, the available data has been interpreted as incompatible with a mid-Ediacaran rifting of RPC from the eastern margin of Laurentia (Rapalini et al., 2015). Despite this progress on the Ediacaran apparent polar wander path of the Río de la Plata craton that has placed some constraints on its paleogeographic evolution and the timing and kinematics of Western Gondwana assembly (e.g. Rapalini, 2018; Rapalini et al., 2021), the paleomagnetic database is still scarce for robust and precise paleogeographic reconstructions.

In order to provide better constraints on the paleogeographic and paleoenvironmental evolution of the southern Río de la Plata craton during Ediacaran times, a multidisciplinary study was initiated by collaboration between researchers of the University of Buenos Aires, National University of La Plata and University of São Paulo on the sedimentary cover of the Tandilia system. The first results of this collaboration are here presented in the form of two companion papers, reporting paleomagnetic, rock magnetic, magnetic stratigraphy and isotope stratigraphy data for the Avellaneda Formation. The present paper is the first one, and describes in detail the paleomagnetic and rock magnetic study carried out on nearly-two hundred and fifty oriented samples of the Avellaneda Formation, mainly from three drill cores drilled near the city of Olavarría, in the Buenos Aires province. Preliminary data from the younger Cerro Negro Formation are also presented. These results permit to determine two new paleomagnetic poles for the Rio de la Plata craton at approximate ages of 570 and 550 Ma providing new evidence on the paleogeography of this cratonic unit during Gondwana assembly.

2. The Tandilia System

The Tandilia System (Fig. 1) is exposed along a 300 km long NW-SE belt in the Buenos Aires province, in central eastern Argentina. The oldest rocks are represented by gneiss, migmatites, granitoids and dykes of the Paleoproterozoic Buenos Aires Complex (Marchese and Di Paola, 1975; Cingolani et al., 2002). The basament rocks were intruded by a swarm of Mesoproterozoic tholeiitic dykes (Teixeira et al., 2002 and references therein) and covered by a Neoproterozoic sedimentary succession of unmetamorphosed and weakly deformed clastic and carbonate rocks. These have been subdivided into the Sierras Bayas (see Poiré and Gaucher, 2009) and La Providencia Groups (Arrouy et al., 2015). The Sierras Bayas Group is made up of the following units, from the oldest to the youngest: Villa Mónica (dolostones and quartzites), Colombo (diamictite), Cerro Largo (sandstones and mudstones), Olavarría (mudstones) and Loma Negra (limestones) Formations (Fig. 2a). The youngest formation of the Sierras Bayas Group, the Loma Negra Formation (Borrello, 1966), consists of a sequence of approximately 40 m of reddish and black micritic limestones deposited in an outer ramp environment under low energy conditions related to a connected ocean, interpreted as Clymene, by suspension fall-out (Gómez-Peral et al., 2019). Gómez-Peral et al. (2007; 2018; 2019) suggested an age between 580 and 590 Ma for this formation on the basis of $\delta^{13}C$ (+2.2 to + 4.5 ‰) and $^{87}Sr/^{86}Sr$ (0.7064 up to 0.7080). In addition, this unit was related to a global oceanic oxygenation event (OOE) at ≃580 Ma (Sahoo et al., 2016) revealed in Loma Negra Formation by redox sensitive indicators (Gómez-Peral et al., 2019). A major regression marks the end of the Sierras Bayas Group, with the development of the erosive Barker surface (Poiré et al., 2007) on the Loma Negra limestones. This big drop in sea-level has been assigned to the Gaskiers glaciation (Gómez-Peral et al., 2018; Poiré et al., 2018), recorded at 580 Ma in Newfoundland (Pu et al., 2016). This surface has been correlated with similar features in other regions of southwestern Gondwana, like in Uruguay, Brazil, South Africa, and Namibia (Poiré et al., 2018 and references therein).

Arrouy et al. (2015) proposed a new stratigraphic scheme for the Late Neoproterozoic cover of the Tandilia system based on the subsurface recognition of a sedimentary succession of 150 m of shales and siltstones. The succession on top of the Barker Surface was included into the La Providencia Group, which is integrated from base to top by the Avellaneda, Alicia and Cerro Negro Formations (Fig. 2a). The Avellaneda Formation (Arrouy et al., 2015) is deposited directly on the erosive Barker Surface. It consists of an association of facies, starting from the base with a mixed composition of massive and laminated marls, increasing the siliciclastic content towards the top where it is composed of massive red clays. The palaeoenvironment proposed for its deposition is intermareal to supramareal, with sparse evidence of subaerial exposure (Arrouy et al., 2015). The age of the Avellaneda Formation is restricted stratigraphically between the Barker Surface and the Late Ediacaran fossils found in the Cerro Negro Formation (see below). This suggests the Avellaneda Formation to be constrained somewhat between 580 Ma and 560 Ma. Accordingly, the carbon isotope profile of the Avellaneda Formation displays a marked negative excursion from + 2.8 to −3.6 ‰, which was considered the cooling response during a post Gaskiers glaciation event (Gómez-Peral et al., 2018; Arrouy et al., 2021) correlated to the onset (574–570 Ma) of the global Shuram carbon isotope excursion (570–562 Ma Gong and Li, 2020; 574-567 Ma Rooney et al., 2020; see Afonso et al., 2022 companion paper).

The Alicia Formation (Arrouy et al., 2015; Arrouy and Gómez-Peral 2021) consists of a clastic succession of black shales in the lower levels that grade into a succession of heterolytic facies of black to grey siltstones and sandstones, both with wavy and lenticular stratification. Massive gray siltstones appear towards the top of the unit. A distal subtidal setting, with anoxic to suboxic conditions, has been inferred for this unit based on its dark color and the presence of pyrite, and later confirmed based on geochemical redox-sensitives indicators (Arrouy and Gómez Peral, 2021).

The Cerro Negro Formation (Iñiguez and Zalba, 1974), redefined by Arrouy et al. (2015), consists of a succession of massive, fine- to medium-grained sandstones with symmetric waves and swaley cross lamination, black to gray heterolytic facies with wavy stratification, and massive red shales. This formation is assigned to a subtidal to intertidal zone with frequent structures associated with tractive processes alternating with subordinate processes of decantation by suspension. Arrouy et al. (2016) reported discoidal structures in fine sandstones of this formation that were assigned to the genus *Aspidella sp*. The characteristics of these fossil remains in the upper levels of the Cerro Negro Formation have been interpreted as corresponding to the "White Sea" Assemblage (Arrouy et al., 2016), with a most probable age between 558 and 550 Ma (Cracknell et al., 2021).

3. Methodology

3.1. Outcrop sampling

The outcrop sampling was carried out in the "La Cabañita" quarry (Cementos Avellaneda SA), near Olavarría city (Fig. 1a). The outcrop consists of a fairly monotonous succession of purple marls with intercalations of lighter levels (Fig. 3a, b). We collected four oriented cores using a portable drill and five oriented hand samples (Site AV1: 36.988780° S, 60.220840° W, Fig. 1b). Whenever possible, samples were oriented with both sun and magnetic compasses. The sampled stratigraphic thickness was just over 6 m.

3.2. Drill core sampling

A detailed study of the Avellaneda Formation was carried out in samples from three vertical drill cores (E34, E7 and H9, Fig. 1b and 2b). Sections of these cores have already been studied for their sedimentological and isotopic aspects by Arrouy et al. (2015) and Gómez-Peral et al. (2018), respectively. Segments of these drill core samples, approximately 10–30 cm in length, were selected for paleo magnetic sampling (see Fig. 3). From each sample, between three to seven

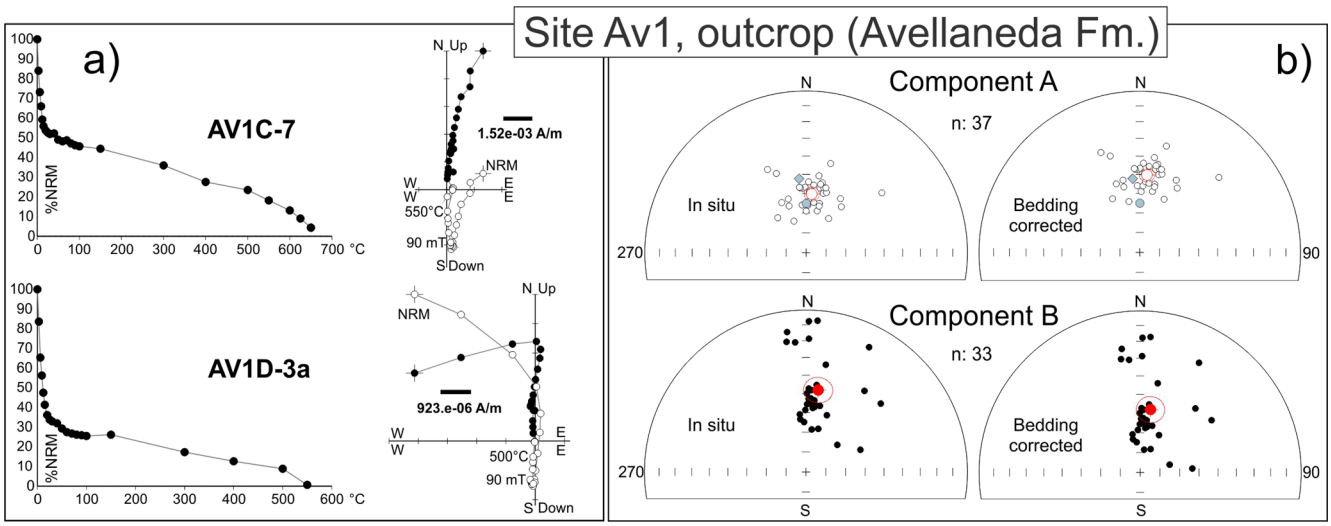

Fig. 4. a) Representative specimens of the Avellaneda Formation at site AV1 demagnetized by alternating fields plus high temperatures. Demagnetization plots and Zijderveld diagrams are shown. In the latter open (full) symbols correspond to projection in the vertical (horizontal) plane; b) Stereographic projections of the specimens directions obtained from the low coercivity component "A" and the high temperature component "B". Blue circle: the direction of the geocentric axial dipole field at the study locality; blue diamond, present geomagnetic field at the study area. Open (full) circles represent upward (downward) directions. The components are shown in "in situ" coordinates and after bedding correction. (For interpretation of the references to color in this figure legend, the reader is referred to the web version of this article.)

cylindrical cores 2.54 cm in diameter and approximately 3 cm in height were extracted, from which a specimen of 2.2 cm high was obtained (Fig. 3). The core segments were drilled centered on the fiduciary mark, which allowed defining their × and y axes. Since the dip of the lamination could be observed and measured along the samples, the relative orientation of the core fiduciary mark was determined with respect to this structural feature. This made possible to azimuthally orient the samples spatially assuming a bedding strike equivalent to the mean strike observed at the nearby AV1 site. This first orientation was later improved using the low-temperature natural remanent magnetization (NRM) component (see section below).

3.2.1. *Drill core E34 (Avellaneda Formation)*

The drill core E34 (Fig. 2b) is located approximately 260 m SSE of the AV1 site, (36.991059° S, 60.220154° W, Fig. 1b). It consists of a succession of massive red marls with some grey color alternations. In the upper half of the profile there are intercalations of massive levels of clays with reddish tones (Fig. 2b). The measured vertical thickness of the Avellaneda Formation in this core is 9 m, extending from 91 m to 82 m below the surface (mbs). Sixteen samples were selected in this drill core (Fig. 3c, d, e). Dipping of the lamination was measured in the laboratory, on each sample fragment. Dip values ranged between 14° and 23°, obtaining an average of 15° for the drill core.

3.2.2. *Drill core H9 (Avellaneda Formation)*

Drill core H9 (Fig. 1b, 36.990898° S, 60.211683° W) is located just over 750 m east of drill core E34. Thickness of the Avellaneda Formation at this drill core reaches 19.7 m, with its base at 77.7 m. and its top at 57.6 m (mbs). It consists of a succession dominated by reddish marls, with a change into a succession of massive shales with red and gray tones in the upper 7 m (Fig. 2b). Thirty-one samples were collected from this drill core (Fig. 3f, g). Lamination is sub-horizontal.

3.2.3. *Drill core E7 (Avellaneda and Cerro Negro Formations)*

Drill core E7 (Fig. 1b, 36.99017° S, 60.228392° W) is located just over 740 m to the west from E34 drill core. The succession belonging to the Avellaneda Formation consists almost exclusively of marls, being mostly reddish, with few intercalations of massive reddish shales (Fig. 2b). The vertical thickness determined for the Avellaneda Formation is 18.3 m, with its base at 57.9 m and its top at 39.7 m (mbs). Twenty-seven samples were collected from this formation (Fig. 3h, i, j). The average dip determined for the laminations is 17°, ranging between 14° and 24°.

Over the Avellaneda Formation there is a very thin level (1.5 m) of the greenish to greyish siliciclastic mudstones of the Alicia Formation, which is overlain by the Cerro Negro Formation. The later consists of reddish heterolithic facies of fine sandstones and shales. The shales show parallel lamination and the sandstones wave ripples and swaley stratification (Fig. 2b). It has a vertical thickness of 7.1 m (between 36.9 and 29.8 m mbs). Ten samples were collected from this formation (Fig. 3k, l). These sediments show an average dip of the lamination of 17°, identical to that measured in the underlying Avellaneda Formation. Dip values ranged between 14° and 21°.

3.3. *Laboratory procedures*

Bulk magnetic susceptibility (k) and k vs temperature curves were performed using a Kappabridge MFK1-A (AGICO) susceptibility-meter with CS-L and CS3 devices. These instruments are located at the "Daniel A. Valencio" Paleomagnetism Laboratory (IGEBA) of the University of Buenos Aires. Hysteresis loops, IRM (isothermal remanent magnetization) and IRM back-field curves were performed using a Molspin ltd. vibration sample magnetometer (VSM) and the paleomagnetic processing of the AV1 site samples using a 2G-550R-DC cryogenic magnetometer, at the same institution. A single chamber ASC48-TD furnace was used for the thermal demagnetization stages, meanwhile a 2G static 3 axes alternating field (AF) demagnetization attached to the cryogenic magnetometer was used for AF demagnetization. Paleomagnetic processing of all drill core samples was conducted at the Laboratory of Paleomagnetism of the University of São Paulo (USPmag), using a cryogenic long-core magnetometer 2G 755–4 K and an ASC48-TD furnace for thermal desmagnetization. Another batch of hysteresis cycles, IRM and IRM back-field curves were performed in this laboratory using a MicroMag-VSM, Model 3900 (Princeton Measurements Corporation).

Table 1
Mean directions per sample with n (specimens) ≥ 3 obtained for the Avellaneda Formation in drill cores H9, E34, E7 and site AV1. N: number of samples; n: number of specimens considered in each sample; NPS: normal polarity specimens; Dec: declination; Inc: Inclination; Lat: latitude; Long: longitude; α_{95} and A_{95}: confidence ellipses for mean directions and VGPs at 95 % confidence, respectively. All normal directions were inverted for the calculation of the mean. All the values in the table are expressed in (°).

		In situ							Bedding corrected					
Sample	NPS	Dec	Inc	α_{95}	n	Lat	Long	A_{95}	Dec	Inc	α_{95}	Lat	Long	A_{95}
H9-11		17.1	59.7	33.3	4	10.9	312.9							
H9-17		14.0	55.3	7.6	3	16.0	311.6							
H9-18		24.0	61.5	4.9	6	7.4	317.4							
H9-19	1	11.8	58.2	6.2	4	13.4	309.2							
H9-20		34.2	63.2	5.4	4	2.7	323.4							
H9-21		16.5	59.7	7.6	5	11.0	312.5							
H9-25		344.6	26.4	21.9	3	37.0	281.0							
H9-28		45.5	51.5	17.0	5	8.9	337.5							
H9-30		53.1	43.2	18.6	4	10.3	347.2							
H9-32		65.7	41.2	19.8	3	3.4	356.6							
H9-4		23.4	63.0	13.8	3	5.8	316.3							
H9-5		2.9	62.1	14.2	4	9.6	301.9							
H9-7		9.7	71.1	7.1	4	−3.0	305.3							
H9-8		30.7	65.5	12.7	4	1.0	319.9							
All (N: 14)	**All (n: 1)**	**24.4**	**58.1**	**8.8**	**56**	**10.0**	**318.5**	**10.3**						
E34-10		12.6	58.3	7.2	4	13.2	309.8		16.3	73.2		−6.8	308.2	
E34-11		20.7	63.0	5.4	5	6.4	314.5		34.8	77.3		−16.2	313.9	
E34-12		16.9	69.6	5.6	3	−1.5	309.8		39.1	84.0		−27.5	308.2	
E34-13		28.3	55.6	13.6	3	12.3	322.9		41.3	69.1		−6.5	323.6	
E34-14	3	39.5	58.0	17.1	3	6.0	329.7		59.9	69.4		−13.9	332.2	
E34-15	2	23.6	58.9	12.2	5	10.3	318.0		36.1	72.9		−10.0	318.1	
E34-16	4	26.5	56.4	16.2	4	12.1	321.2		39.0	70.1		−7.1	321.6	
E34-1		22.4	49.7	6.8	5	19.3	320.1		29.6	63.9		3.2	320.0	
E34-2		17.4	47.6	6.6	4	22.3	316.3		21.7	62.4		6.9	315.4	
E34-4	2	17.4	61.4	45.4	3	8.9	312.7		26.7	75.9		−12.6	311.7	
E34-5		357.6	44.7	14.8	3	26.6	297.4		353.3	59.3		12.7	294.5	
E34-6		6.2	37.6	4.0	3	31.7	306.6		5.6	52.6		19.6	304.8	
E34-7		2.4	42.4	1.9	4	28.4	302.3		0.4	57.3		15.1	300.1	
E34-8		8.6	42.3	7.0	6	28.0	308.7		8.8	57.3		14.7	307.0	
E34-9		13.0	53.2	4.7	3	18.2	311.1		16.1	68.1		0.7	309.8	
All (N: 15)	**All (n: 11)**	**15.7**	**53.7**	**5.3**	**58**	**16.3**	**313.7**	**6.0**	**20.5**	**68.5**	**5.3**	**−1.9**	**312.7**	**8.0**
E7-11		352.2	61.3	8.6	5	10.3	293.9		25.6	64.7		3.3	317.1	
E7-12		349.0	52.2	10.0	3	19.5	290.0		12.4	58.0		13.5	309.7	
E7-13		345.9	54.2	10.0	3	17.1	287.7		11.0	60.6		10.8	308.1	
E7-14		317.2	62.1	12.2	3	0.7	270.2		346.7	75.1		−9.6	293.5	
E7-15		332.5	65.1	8.0	3	2.9	281.5		13.6	73.3		−6.7	306.8	
E7-20		347.8	45.6	15.1	4	2.4	287.8		6.0	52.4		19.8	305.1	
E7-21		334.1	64.5	6.7	6	3.5	282.2		14.0	72.5		−5.5	307.2	
E7-22		353.6	68.3	11.8	3	1.4	295.8		39.1	69.5		−6.4	322.1	
E7-23		327.7	59.3	8.1	3	7.4	275.4		356.8	70.2		−1.3	297.9	
E7-26	1	357.4	55.6	15.9	5	16.8	297.6		23.7	58.5		10.7	318.3	
E7-36	3	265.2	81.7	5.8	3	−36.6	279.4		130.3	79.9		−47.8	322.1	
E7-37		345.7	63.6	7.0	7	6.8	289.7		23.5	68.4		−1.0	314.1	
E7-38		344.7	70.8	8.6	4	−3.1	291.1		39.4	73.5		−11.7	319.1	
E7-40	2	273.9	80.2	13.5	3	–33.4	276.8		130.0	82.0		−45.9	317.1	
E7-42	1	348.9	66.2	17.9	3	3.9	292.4		31.2	69.4		−4.0	318.0	
E7-43	3	300.5	72.4	7.9	3	−16.9	270.9		15.1	86.9		−31.0	301.7	
E7-44	3	271.5	86.8	14.3	3	−36.6	291.8		114.2	76.0		−43.2	333.7	
E7-45	6	234.5	70.0	10.5	6	−49.4	252.3		182.5	72.8		−68.7	296.2	
All (N: 18)	**All (n: 19)**	**335.5**	**68.1**	**6.7**	**70**	**−3.0**	**284.4**	**10.7**	**24.5**	**74.5**	**6.7**	**−12.0**	**311.6**	**11.6**
AV1A		359.3	17.4	8.3	7	44.1	298.8		358.9	27.4		38.5	298.4	
AV1C		4.8	55.5	2.7	10	16.8	303.8		4.7	65.5		5.3	303.0	
AV1D		1.7	54.1	5.0	8	18.4	301.3		0.5	64.1		7.2	300.1	
AV1E		27.1	61.3	14.3	5	6.9	319.6		37.3	70.2		−6.7	320.7	
All (N: 4)	**All (n: 0)**	**6.1**	**47.8**	**25.0**	**30**	**21.6**	**306.5**	**21.0**	**6.4**	**57.8**	**25.0**	**11.0**	**305.9**	**25.3**
All (N: 51)	**All (n: 31)**	**7.0**	**60.9**	**4.8**	**214**	**8.7**	**304.3**	**6.6**	**21.4**	**67.1**	**4.2**	**−1.0**	**313.4**	**5.9**

4. Paleomagnetic results

4.1. Site AV1

Samples from AV1 site were submitted to a first stage of demagnetization by alternating magnetic fields (AF) in steps of 3, 6, 9, 12, 15, 20, 25, 30, 40, 50, 60, 70, 80 and 90 mT, followed by a second stage of high temperature demagnetization in steps of 100, 150, 300, 400, 500, 530, 560, 590, 620 °C. Each sample demagnetization behavior was analyzed independently and prIncipal component analysis (PCA, Kirschvink, 1980) was used to determine the magnetic components. A "soft" magnetic component, labelled "A", with low to medium coercivities was defined at alternating magnetic fields under 40 mT. Between 50 and 90 mT very little remanence was removed. The characteristic remanent magnetization (ChRM or component "B") could be defined by high-temperature demagnetization at ranges higher than 150–200 °C, showing a trend towards the origin of coordinates in Zijderveld diagrams. In some cases, unblocking temperatures close to or greater than 600° C were observed, while in other samples the unblocking temperatures were lower, between 500 and 550° C (Fig. 4a). "In situ" mean

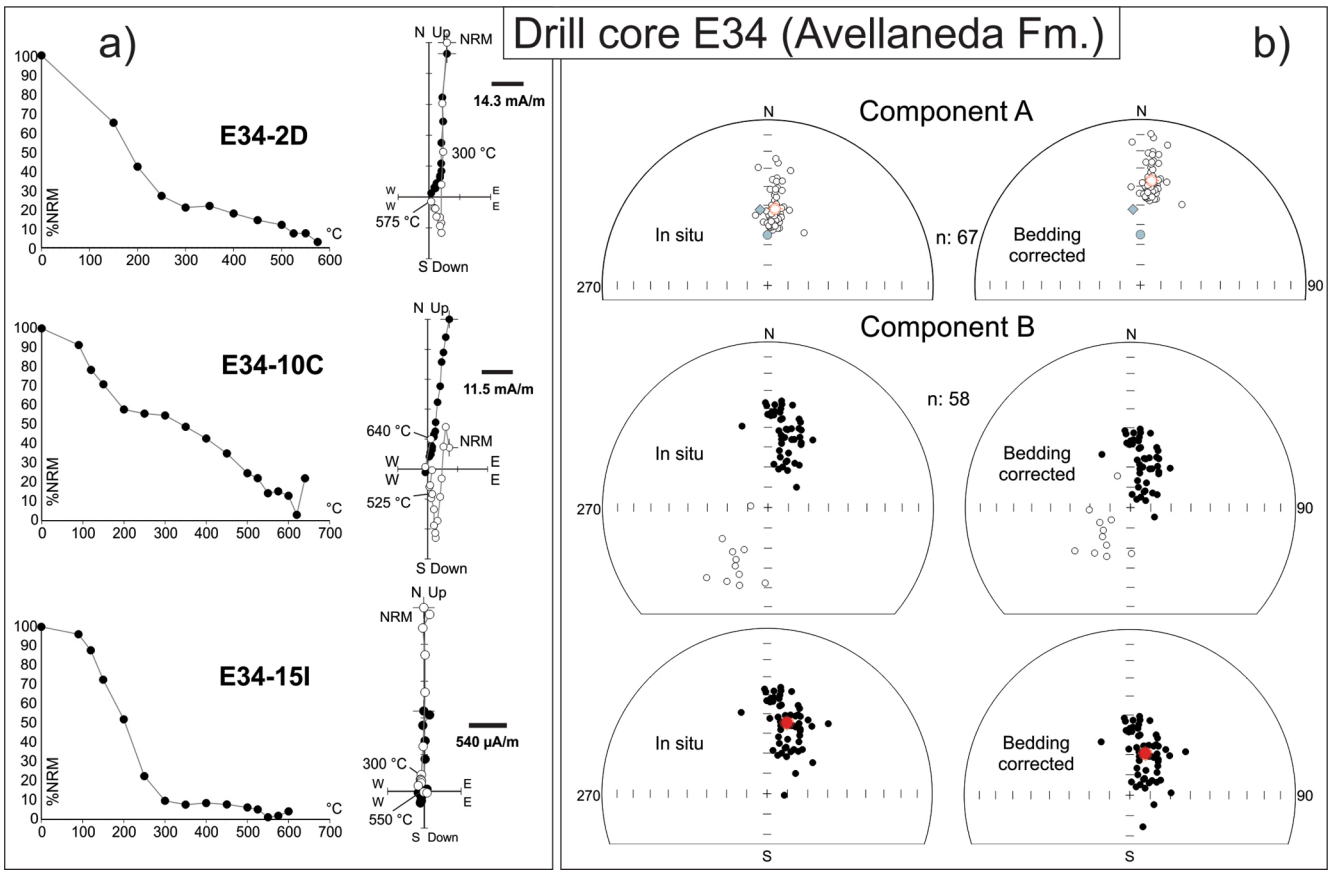

Fig. 5. a) Representative specimens of the Avellaneda Formation in E34 drill core demagnetized by high temperatures. Demagnetization plots and Zijderveld diagrams are shown; b) Stereographic projections of the specimen directions obtained from the low coercivity component "A" and the high temperature component "B". Blue circle: the direction of the geocentric axial dipole field at the study locality; blue diamond, present geomagnetic field at the study area. The components are shown in "in situ" geographic coordinates and after bedding correction. Lowermost stereonet shows specimen ChRM directions after inverting those of negative inclinations. References as in Fig. 4. (For interpretation of the references to color in this figure legend, the reader is referred to the web version of this article.)

direction of component "A" was Dec: 5.5°, Inc: −60.2°, α_{95}: 3.6°, k: 43.4, n: 37 (specimens) (Fig. 4b). Component "B", interpreted as the characteristic remanent magnetization, presented a consistent direction in the analyzed specimens, with moderate to high positive Inclinations, pointing to the north, obtaining a mean "in situ" direction of Dec: 8.5°, Inc: 47.6°, α_{95}: 6.9°, k: 14.3, n: 33 (specimens). After application of the bedding correction, the characteristic mean direction for"B" at AV1 is Dec: 9.5°, Inc: 57.6°, α_{95}: 6.9°, k: 14.3 (Fig. 4b, Table 1 and 4).

An analysis of great circles (MacFadden and McElhinny, 1988) was carried out for specimens from the hand sample AV1A, sInce their components "B" show lower Inclinations than the remaining specimens in the AV1 site. We found that the great circle intersection in geographic coordinates was Dec: 359.2°, Inc: 25.4°, α_{95}: 5.9° while the mean direction obtained for component "B" using PCA analysis was Dec: 359.3°, Inc: 17.4°, α_{95}: 8.3°; n: 7. After bedding correction, the great circle intersection is at Dec: 358.5°, Inc: 35.3°, meanwhile component "B" mean direction from PCA was Dec: 358.9°, Inc: 27.4°. The difference between mean Inclinations (~8°) computed in both ways suggests that minor contamination of component "B" directions by component "A" is possible.

4.2. Drill core E34

Sixteen samples were collected from this drill core. The measured vertical thickness for the Avellaneda Formation was ~ 9 m (Fig. 2). All paleomagnetic specimens (n: 58) were demagnetized with high temperatures according to the following steps: 90, 120, 150, 200, 250, 300, 350, 400, 450, 500, 525, 550, 575, 600, 620 and 640 °C. (Fig. 5a). The behavior during thermal demagnetization was very similar in all specimens. Up to approximately 250–350 °C, a NW to NE directed magnetic component (component "A") of moderate negative Inclination was isolated. The maximum angular deviation (MAD) values were always below 12°. This component was used to refine the azimuthal orientation of the sampled fragments of the core, previously oriented assuming same dip direction of the lamination as in the outcrop site AV1. As a reference for this "second step" of azimuthal orientation, we used component "A" isolated in the specimens obtained in the outcrops of the quarry (site AV1) (see Fig. A1 in the appendix section to see specimens directions before azimuthal correction). To achieve that we rotated the "A" in situ mean direction for each core sample around a vertical axis so that its mean declination matches that obtained for the same component at site AV1 (Dec: 5.5°). After this we were able to determine with more confidence the dip direction of the layers observed in the core (Az = 188°), in order to perform a more reliable bedding correction. Fig. 5b shows the directions of component "A" isolated from each specimen "in situ" (after this azimuthal correction) and after bedding correction (mean dip 15° towards Az: 188°). The average of these directions "in situ" is: Dec: 5.5°, Inc: −51.6°, k: 69.2, α_{95}: 2.1°, n: 67, while corrected to the paleohorizontal is: Dec: 6.0°, Inc: −36.7°, k: 69.2, α_{95}: 2.1°. SInce assuming a Fisherian distribution in this case is not strictly valid, because the mean direction of the sample was pre-determined to be of declination 5.5°, a mean Inclination only computation was carried out for components "A" of this drill core (McFadden & Reid, 1982). In this way, in geographic coordinates, the "A" component mean Inclination was −51.5°, k: 38.3, α_{95}: 2.6°, n: 67 while after bedding correction it turned out −36.6°, k: 38.5, α_{95}: 2.4°. Between 350 and 575 °C component "B" was isolated,

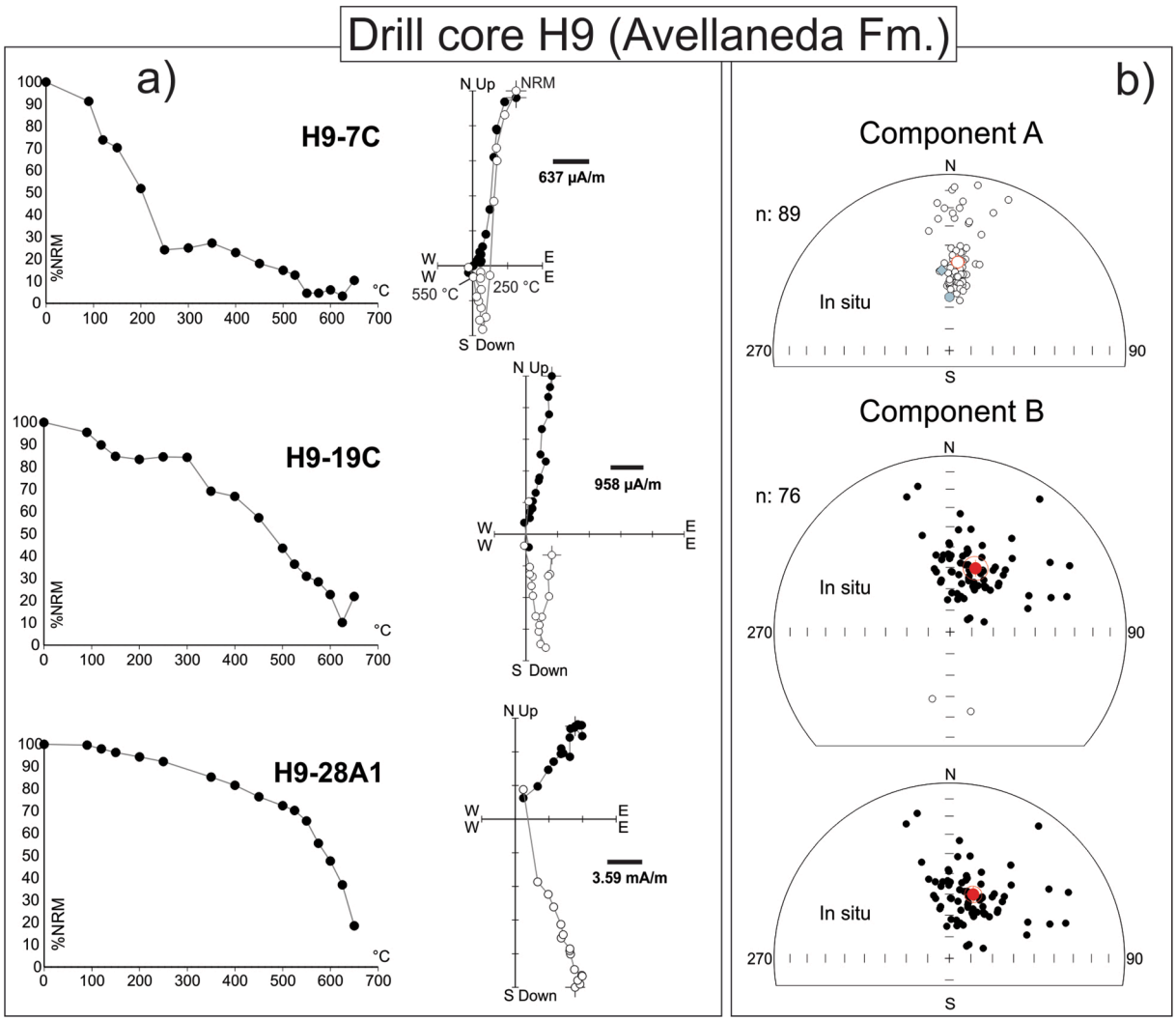

Fig. 6. a) Representative specimens of the Avellaneda Formation in H9 drill core demagnetized by high temperatures. Demagnetization plots and Zijderveld diagrams are shown; b) Stereographic projections of the specimen directions obtained from the low coercivity component "A" and the high temperature component "B". Blue circle: the direction of the geocentric axial dipole field at the study locality; blue diamond, present geomagnetic field at the study area. The components are shown only in "in situ" geographic coordinates as bedding is horizontal. Lowermost stereonet shows specimen ChRM directions after inverting those of negative inclinations. References as in Fig. 4. (For interpretation of the references to color in this figure legend, the reader is referred to the web version of this article.)

generally trending towards the origin of coordinates (Fig. 5a). Maximum accepted MAD was of 15°, but most (80 %) were less than 10°. The minimum number of demagnetization steps to determine components was 6. At temperatures of 600° C or higher all specimens showed an abrupt Increase in the intensity of magnetic remanence and random directions. At this temperature, they also presented an Increase in bulk magnetic susceptibility, sometimes of one order of magnitude. Forty-seven specimens showed a ChRM pointing NNE and downwards, while eleven specimens (from samples E34-14, E34-15 and E34-16) presented nearly antipodal, SSW and upwards directions. Component "B" "in situ" mean direction is: Dec: 15.7°, Inc: 53.3°, α_{95}: 3.2°, k: 35.4, n: 58 and after bedding correction: Dec: 20.4°, Inc: 68.1°, α_{95}: 3.2°, k: 35.4 (Fig. 5b, Table 1 and 4). It is interesting to note that the mean bedding-corrected direction of component "B" is very similar to that of the same component determined at AV-1. None of these two mean directions are similar to any expected post-Cambrian directions for the study area (e.g. Torsvik et al., 2012).

4.3. Drill core H9

Thirty-one samples were collected from this drill core, where the measured vertical thickness for the Avellaneda Formation was 19.7 m (Fig. 2). The paleomagnetic processing consisted of high-temperature demagnetization following the same steps as in the previous case. A low temperature component "A" was isolated at temperatures below 200-300° C in most specimens. A second component "B" of high unblocking temperature was generally determined between 350 and 575° C, or up to 600° C in some cases (Fig. 6a). In this collection, all except two specimens showed a NW to NE downward directed ChRM. The demagnetization behavior was very similar to that observed in samples from drill core E34. Unlike the other two cores, the H9 presented subhorizontal laminations. Azimuthal orientation of the samples was therefore only achieved by rotating each sample around a vertical axis so that the component "A" mean sample declination coIncides with that obtained for the same component at AV-1. The mean direction of component "A" is, Dec: 5.4°, Inc: −48.2°, α_{95}: 2.8°, k: 28.9, n: 89. The

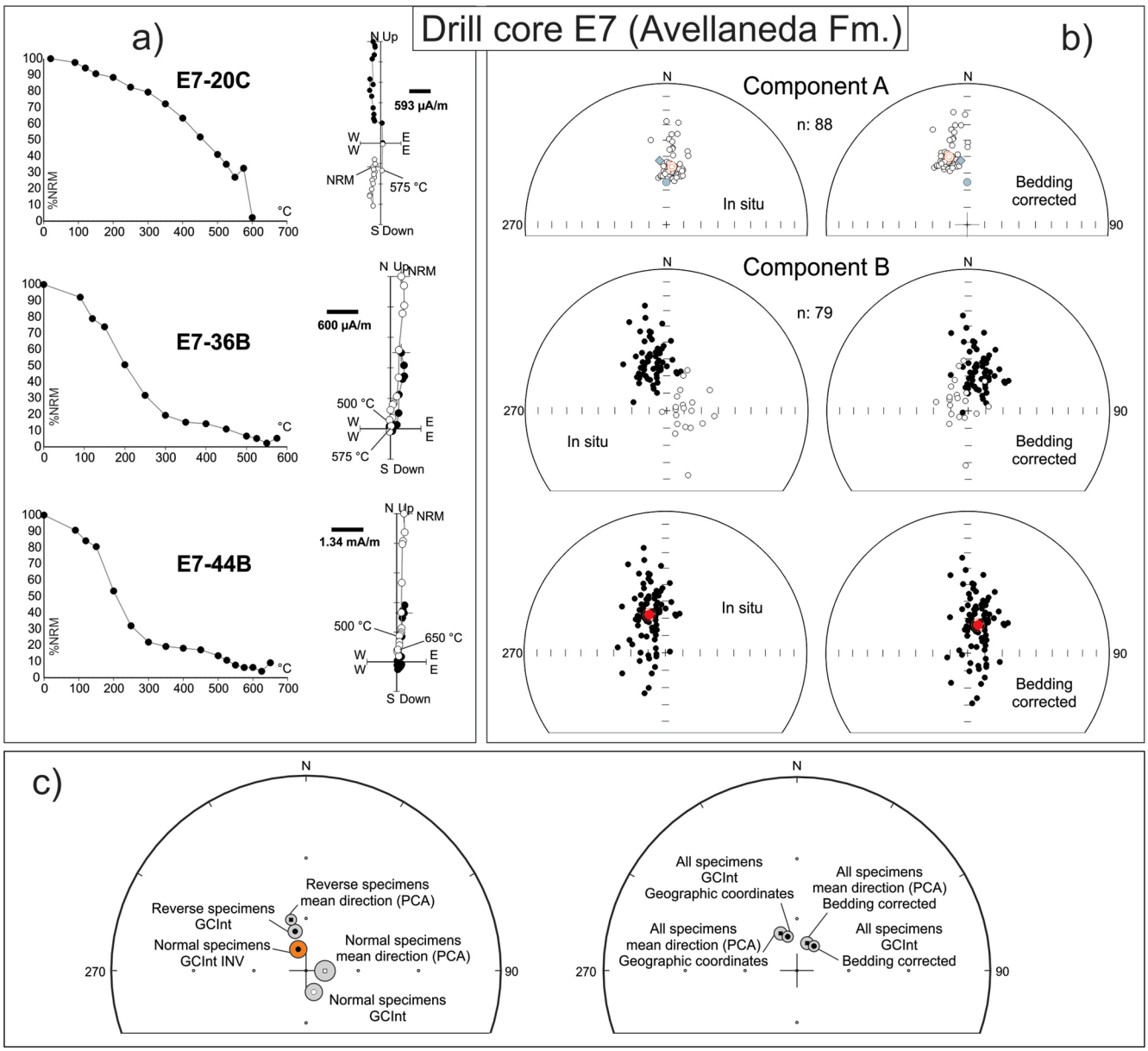

Fig. 7. a) Representative specimens of the Avellaneda Formation in E7 drill core demagnetized by high temperatures. Demagnetization plots and Zijderveld diagrams are shown. b) Sterographic projections of the specimens directions obtained from the low coercivity component "A" and the high temperature component "B". Blue circle: the direction of the geocentric axial dipole field at the study locality; blue diamond, present geomagnetic field at the study area. Components are shown in "in situ" geographic coordinates and after bedding correction, lowermost stereonet shows specimen ChRM directions after inverting those of negative inclinations; c) In the left, the stereographic projections of great circle intersections for specimens with ChRM of positive and negative inclinations directions, and the mean directions for the same specimens as obtained by PCA. In red, inverted great circle intersection of the negative inclination ChRM. In the right, great circle intersections and mean directions for all specimens from drill core E7 in geographic coordinates and after bedding correction. See section 5.3 for the reversal test analysis. GCInt: great circle intersection; GCInt INV: great circle intersection inverted. References as in Fig. 4. (For interpretation of the references to color in this figure legend, the reader is referred to the web version of this article.)

Inclination only calculation yield an Inclination of −48.1°, α_{95}: 3.7°, k: 15.2, n: 89. Component "B" yielded a mean direction: Dec: 20.5°, Inc: 58.0°, α_{95}: 3.9°, k: 18.3, n: 76 (Fig. 6b, Table 1 and 4).

As illustrated in Fig. 6 b, a group of "A" component directions show anomalous low Inclinations. In order to test whether they were affected by "contamination" with another magnetic component a great circle analysis was performed. Specimens for samples H9-13, H9-15, H9-21, H9-22, H9-25, H9-27, H9-28 and H9-32 were analyzed. In the cases of the specimens from H9-15, H9-27 and H9-32 no great circles could be determined with acceptable precision (MAD less than 15°). From samples H9-21, H9-25 and H9-28 (a total of 11 specimens) great circles were obtained from 90 up to 450 °C (or even 575 °C in one specimen) in the former sample. In the latter two cases, the range was between 90 and 400 °C. A minor overlap between components "A" and "B" cannot be ruled out, from his great circle intersection (Dec: 1.1°, Inc: −27.5, α_{95}: 4.3°; n: 11). On the other hand, samples H9-13 and H9-22 only showed a single specimen with anomalous low Inclinations. Component "B" specimen directions show some scatter with lower Inclinations towards the NNW (H9-25) and E (H9-28, H9-30 and H9-32). However, either no great circles could be determined with acceptable precision or anomalous directions corresponded to isolated specimens (H9-25, H9-28, H9-32). In the case of sample H9-30, only two great circles could be determined between 90 up to 625 °C with an intersection at Dec: 61.3°, Inc: 38.6°. If we considered that the mean direction of component "B"

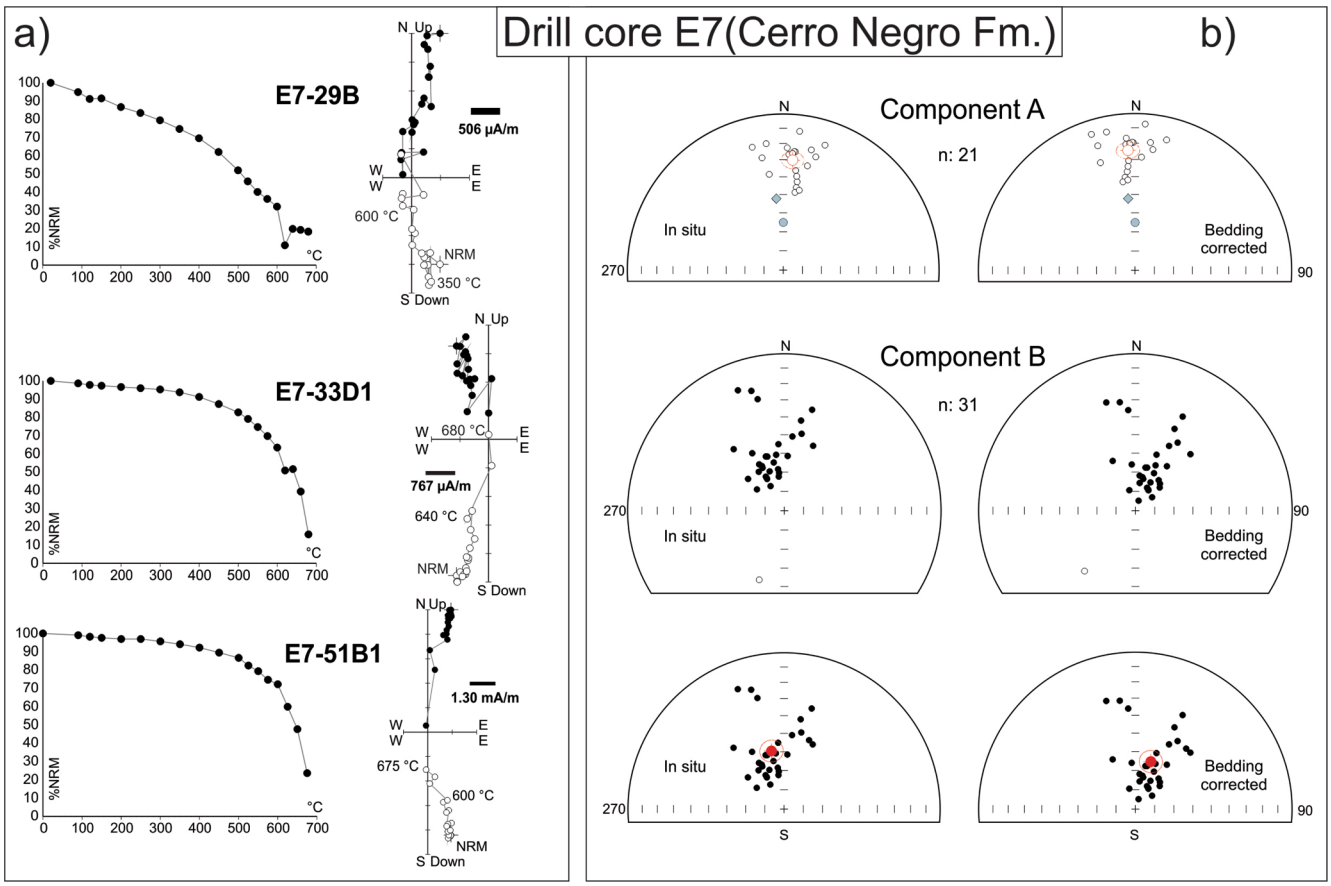

Fig. 8. a) Representative specimens of the Cerro Negro Formation in E7 drill core demagnetized by high temperatures. Demagnetization plots and Zijderveld diagrams are shown; b) Stereographic projections of the specimen directions obtained from the low coercivity component "A" and high temperature component "B". Blue circle: the direction of the geocentric axial dipole field at the study locality; blue diamond, present geomagnetic field at the study area. The components are shown in "in situ" geographic coordinates and after bedding correction. Lowermost stereonets show specimen ChRM directions after inverting a single one of negative inclination. More references in Fig. 4. (For interpretation of the references to color in this figure legend, the reader is referred to the web version of this article.)

Table 2
Mean directions per sample obtained for the Cerro Negro Formation in drill core E7. For references see Table 1. With (*) sites previously reported by Rapalini et al. (2013). All the values in the table are expressed in (°).

	In situ							Bedding corrected					
Sample	Dec	Inc	α_{95}	n	Lat	Long	A_{95}	Dec	Inc	α_{95}	Lat	Long	A_{95}
E7-27	340.5	68.0	7.9	5	0.3	287.7		28.6	73.0		−8.5	314.4	
E7-28	338.9	29.4	18.6	4	33.7	275.2		348.3	39.5		29.6	287.3	
E7-29	352.1	61.2	24.1	2	10.4	293.8		25.4	64.7		3.4	316.9	
E7-30	330.2	62.1	9.0	3	5.2	278.5		4.6	71.7		−3.6	302.3	
E7-31	338.4	71.8	4.7	4	−5.4	288.1		38.8	75.7		−14.7	316.9	
E7-32	14.2	41.1	32.9	2	28.0	314.5		29.0	40.6		23.9	328.9	
E7-33	342.1	67.0	10.3	3	1.9	288.3		27.4	71.9		−6.6	314.5	
E7-34	344.5	59.3	31.3	2	11.6	287.7		15.5	65.3		4.5	310.2	
E7-35	322.4	64.9	20.9	2	−0.4	275.1		1.0	76.1		−10.7	300.2	
E7-51	14.9	49.2	8.5	4	21.5	313.6		34.2	47.8		16.7	330.7	
All (N: 10)	**348.3**	**58.7**	**10.0**	**31**	**10.9**	**290.0**	**11.4**	**18.5**	**63.7**	**10.0**	**3.4**	**312.4**	**12.1**
OV-9*	21.4	40.9	11.8	9	26.3	321.7		37.0	59.2		5.9	327.4	
OL-20*	6.0	46.1	–	1	25.3	305.7		2.4	48.3		23.7	302.0	
OL-21*	327.1	74.3	80.6	2	−11.3	284.0		33.3	49.6		15.7	329.2	
OV-22*	5.9	54.2	27.1	5	17.4	305.7		19.4	53.0		16.5	317.4	
All (N: 4)	**6.8**	**54.8**	**20.9**	**17**	**15.0**	**303.9**	**27.0**	**22.2**	**53.3**	**12.3**	**15.7**	**319.3**	**16.0**
All (N: 14)	**353.9**	**57.9**	**8.5**	**48**	**12.1**	**293.8**	**10.1**	**19.8**	**60.7**	**7.7**	**7.0**	**314.4**	**9.5**

Table 3
Great circles intersections obtained for the Avellaneda and Cerro Negro Formations. For references see Table 1. All the values in the table are expressed in (°).

			In situ				Bedding corrected	
Site/Drill core	Unit	Samples	Dec	Inc	α_{95}	n	Dec	Inc
AV1	Avellaneda	AV1A	359.2	25.4	5.9	8	358.5	35.3
H9	Avellaneda	H9-21	358.1	−52.8	7.3	5	–	–
		H9-22	348.6	−62.3	–	3	–	–
		H9-28	351.5	−36.7	16.1	4	–	–
E7	Avellaneda	Normal polarity	159.9	−76.7	5.0	20	236.1	−76.4
		Reverse polarity	344.4	66.4	4.0	50	27.8	70.8
		All (N: 70)	**344.8**	**69.4**	**3.2**	**70**	**34.9**	**72.5**
E7	Cerro Negro	E7-27	339.1	69.6	13.9	5	32	74.4
		E7-28	319.7	43.9	15.6	4	332.2	54.8
		E7-30	345.9	58.1	–	3	15.4	64.0
		E7-31	325.5	71.5	–	2	29.3	79.2
		E7-32	15.0	46.0	–	2	32.4	44.9
		E7-33	327.0	71.6	–	3	30.8	78.8
		E7-34	264.5	74.2	–	2	178.4	82.8
		E7-35	314.6	71.1	–	2	17.9	82.2
		All samples (N: 8)	**333.4**	**66.0**	**12.4**	**23**	**16.9**	**73.8**
		All specimes (n: 24)	**325.7**	**67.3**	**5.1**	**24**	**12.4**	**76.8**

Table 4
Mean ChRM directions determined for the Avellaneda and Cerro Negro Formations. Mean directions obtained by averaging specimens, by considering sample/site, and samples with specimens ≥ 3 are shown. BP: bedding plane (strike/dip, right hand convention); N: number of samples taken from the drill cores and in the outcrop at AV1; n: number of specimens; Dec: declination; Inc: Inclination; α_{95} and k: Fisherian statistical parameters. All the values in the table are expressed in (°), with the exception of the k parameter. (*) mean Including specimens and samples reported in Rapalini et al. (2013). CNF: Cerro Negro Formation sites previously reported by Rapalini et al. (2013): OV-9, OL-20, OL-21 and OV-22. GC: direction computed with great circle analysis. PCA: direction computed with prIncipal component analysis. In bold, the Avellaneda and Cerro Negro formations directions used to compute paleomagnetic poles.

					Geographic coordinates				Bedding corrected			
Geologic unit	Drill core/outcrop	BP (°)	N	n	Dec	Inc	α_{95}	k	Dec	Inc	α_{95}	k
Avellaneda Fm.	AV1	95/10	5	33	8.5	47.6	6.9	14.3	9.5	57.6	6.9	14.3
	E34	98/15	15	58	15.7	53.3	3.2	35.4	20.4	68.1	3.2	35.4
	H9	0/0	25	76	20.5	58	3.9	18.3	–	–	–	–
	E7	20/17	24	79	336.9	66.1	3.7	19.5	20.5	72.8	3.7	19.5
	All (specimens)	–	–	246	6.6	59.3	2.4	15.1	18.6	65.2	2.2	18.0
	All (samples)	–	69	–	6.5	59.1	4.2	17.3	18.8	64.2	3.9	20.5
	All (samples with n ≥ 3)	**–**	**51**	**–**	**7.0**	**60.9**	**4.8**	**18.3**	**21.4**	**67.1**	**4.2**	**23.9**
Cerro Negro Fm.	E7 (specimens-PCA)	20/17	–	31	347.8	58.8	5.9	20.3	18.2	64.0	5.9	20.3
	E7 (specimens-GC)	20/17	–	24	325.7	67.3	5.1	36.3	12.4	76.8	5.1	36.3
	E7 (samples-PCA)	20/17	10	–	348.3	58.7	10.0	24.4	18.5	63.7	10.0	24.4
	E7 (samples-GC)	20/17	–	8	333.4	66.0	12.4	20.9	16.9	73.8	12.4	20.9
	E7 + CNF (specimens)*	–	–	48	358.8	56.4	5.8	13.8	22.4	61.3	5.1	17.6
	E7 (samples PCA) + CNF (sites)*	–	14	–	353.9	57.9	8.5	23.0	19.8	60.7	7.7	27.7
	E7 (samples GC) + CNF (sites)*	**–**	**11**	**–**	**344.2**	**64.7**	**11.2**	**17.7**	**22.0**	**68.5**	**10.3**	**20.8**

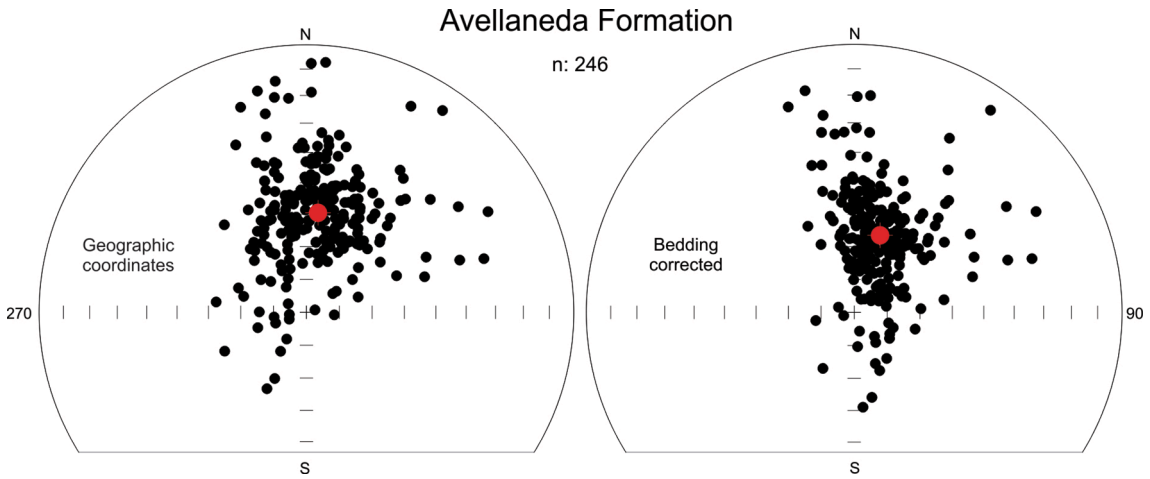

Fig. 9. Stereographic projections of the characteristic remanence directions and the overall mean direction (full red circle) obtained at a specimen level for the Avellaneda Formation. The directions are represented in in situ geographic coordinates (left) and after bedding correction (right). Specimen directions of negative inclinations have been inverted into its antipodal hemisphere. (For interpretation of the references to color in this figure legend, the reader is referred to the web version of this article.)

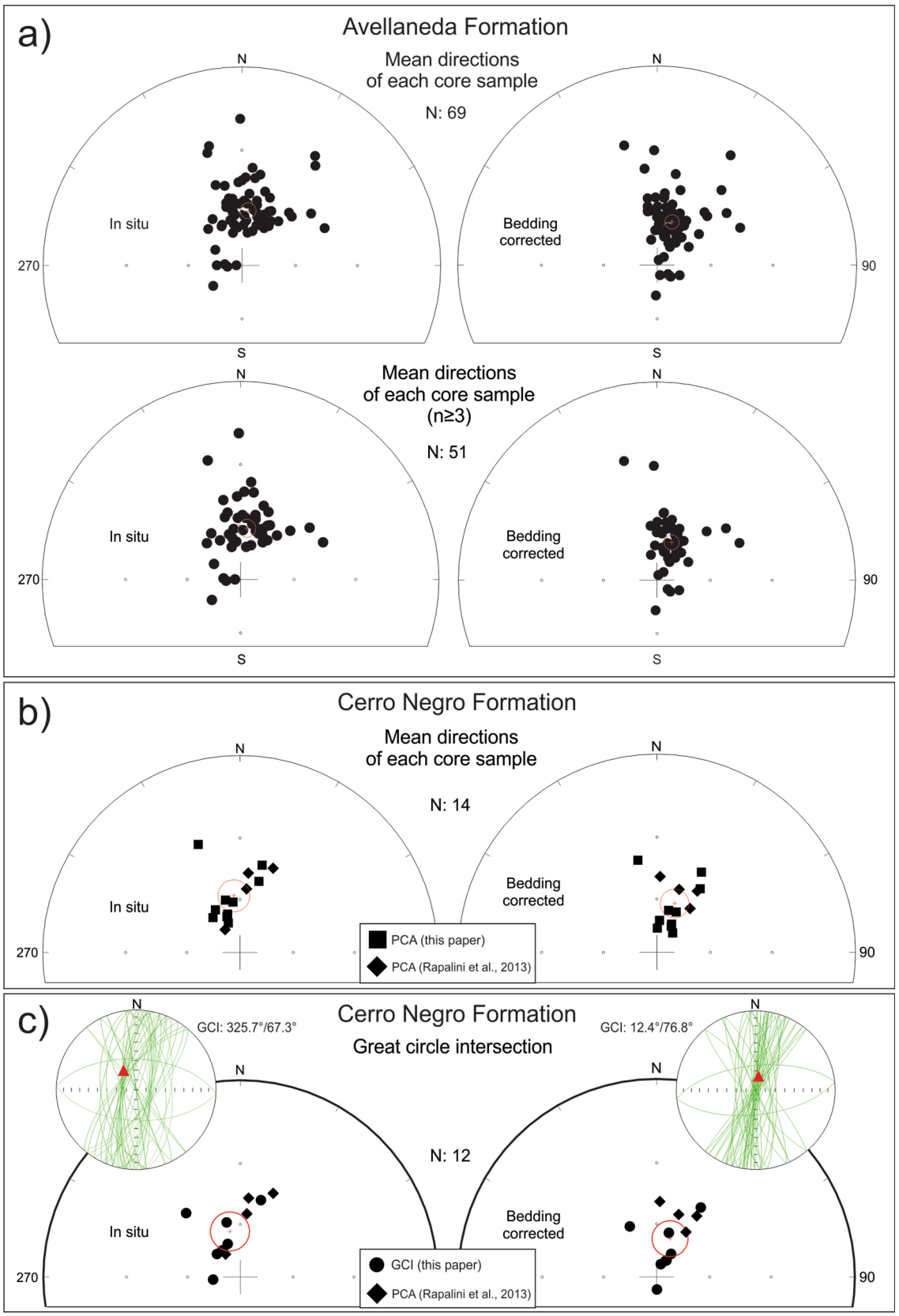

Fig. 10. a) Stereographic projections of the characteristic remanence directions and mean directions obtained for the Avellaneda Formation on a sample basis (upper diagrams), and excluding samples with less than 3 specimens (lower diagrams), in in situ coordinates (left) and after bedding corrections (right); b) idem a) for the Cerro Negro Formation considering all the samples taken from the drill core E7 and those directions reported in Rapalini et al. (2013) (black diamonds); c) Mean great circle intersection of each sample compared with the mean directions reported by Rapalini et al. (2013) in situ and after bedding correction. The great circles of each specimens of the Cerro Negro Formation reported in this paper are also shown. PCA: principal component analysis; GCI: great circle intersection.

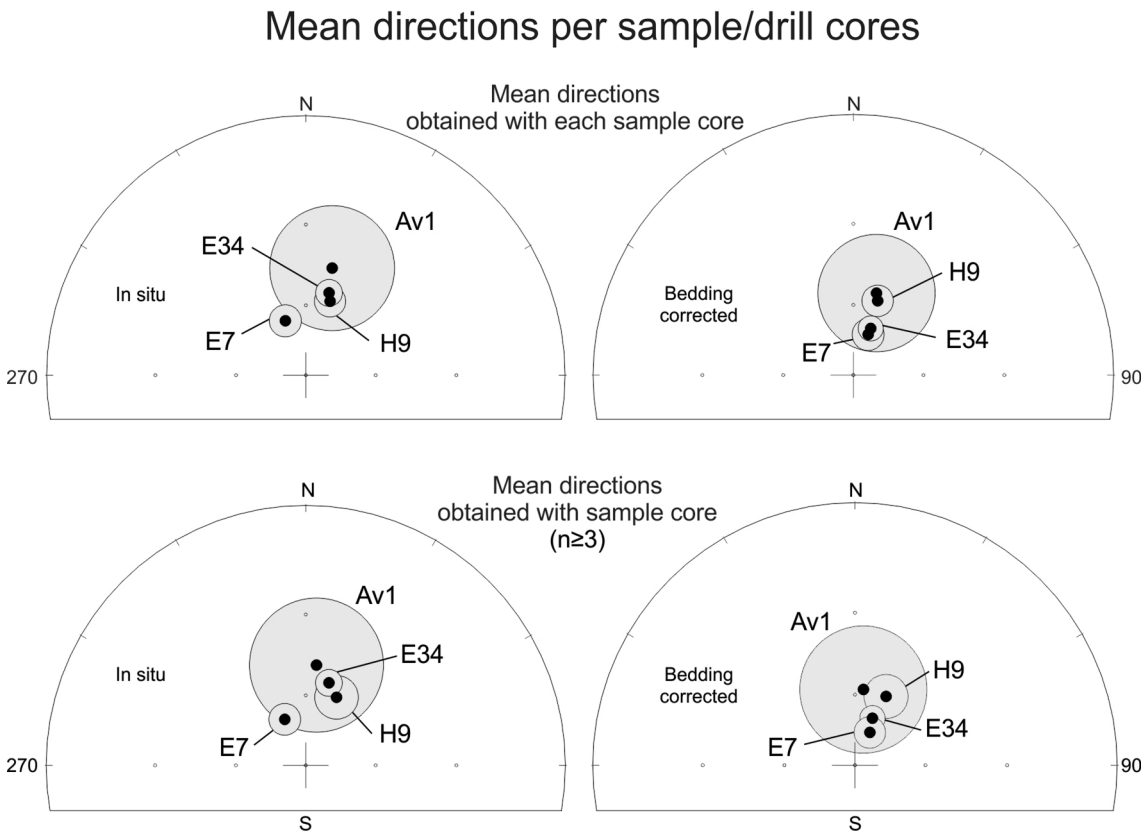

Fig. 11. Stereographic projections of the mean directions obtained per drill core and site AV1 for the Avellaneda Formation. It is analyzed considering all samples and with those samples with n ≥ 3 specimens. The directions are shown in geographic coordinates and after bedding correction.

obtained through PCA from 4 specimens at this sample is Dec: 53.1°, Inc: 43.2°, α_{95}: 18.6°, components overlapping seems unlikely.

4.4. Drill core E7

Twenty-seven samples were collected for the Avellaneda Formation from this drill core. Measured vertical thickness of this unit was 17.5 m. All specimens were demagnetized by high temperatures. Heating steps were the same as those applied to the other drill cores specimens. Component "A" was determined between 100 and 350° C. The high temperature, characteristic component "B" was isolated between 350 and 550° C in most cases. In just few specimens unblocking temperatures reached 575 °C or even 600° C (Fig. 7a). Both polarities of component "B" were recorded. As in E34, in situ mean direction of Component "A" for each sample was used to check and correct the azimuthal orientation of the core, previously obtained by assuming same lamination dip direction than that measured at AV1, by comparison with mean declination of this component at that site. Negative Inclinations were found for Component "B" at samples E7-26, E7-36, E7-40, E7-42, E7-43, E7-44 and E7-45. The measured averaged dip of the laminations was of 17°. The mean direction obtained for Component "A" in "in situ" coordinates is: Dec: 5.4°, Inc: −56.0°, α_{95}: 1.5°, k: 101.1, n: 88 while after bedding correction is Dec: 345.1°, Inc: −48.8°, α_{95}: 1.5°, k: 101.1. The Inclination only mean computed for this component yielded, in geographic coordinates, a value of −55.9°, α_{95}: 1.9°, k: 59.6, n: 88 and after bedding correction −48.6°, α_{95}: 1.5°, k: 67.3. On the other hand, mean direction of Component "B" in"in situ" coordinates is Dec: 336.9°, Inc: 66.1°, α_{95}: 3.7°, k: 19.5, n: 79 while after bedding correction the mean direction is Dec: 20.5°, Inc: 72.8°, α_{95}: 3.7°, k: 19.5 (Fig. 7b, Table 1 and 4).

Fig. 7b shows that component "B" directions are of both positive and negative Inclinations. However, visual inspection of the stereonet clearly indicates that they are not antipodal. When those of negative Inclination are inverted, a conspicuous elongated distribution can be observed. This could be due to partial overprint of component "A" on component "B", not adequately erased during demagnetization. Therefore, a great circle analysis was performed on demagnetization results from all specimens of the Avellaneda Formation at this drill core (n: 70). The analysis consisted in determining great circles trajectories for demagnetization steps higher than 400 °C (the usual lowermost temperature step utilized to isolate component "B" with PCA). Great circle intersection was obtained yielding a direction at Dec: 344.8°, Inc: 69.4°, α_{95}: 3.2°, n: 70 in geographic coordinates. After bedding correction, the intersection is at Dec: 34.9°, Inc: 72.5°, α_{95}: 3.2°. Both of them are very close to the mean directions obtained through PCA. The mean direction in geographic coordinates is Dec: 336.3°, Inc: 66.3°, α_{95}: 3.7°, n: 79 while after bedding correction is Dec: 20.5°, Inc: 72.8°, α_{95}: 3.7°. These close directions found between great circles intersections and mean direction suggest an overlap between components "A" and "B", however, it is not significant enough to change our directional analysis. When the comparison of mean direction from PCA and great circles intersection was made for those of negative Inclination alone, the great circle intersection is Dec: 159.9°, Inc: −76.7°, α_{95}: 5.0°, n: 20 while the mean direction is Dec: 90.7°, Inc: −78.9°, α_{95}: 6.0°, n: 20. With the reversal specimens the great circle intersection is Dec: 344.4°, Inc: 66.4°, α_{95}: 4.0°, n: 50 and the mean direction is Dec: 343.6°, Inc: 59.6°, α_{95}: 3.0°, n: 59 (Fig. 7c) (see section 5.3 for the reversal test analysis).

The Cerro Negro Formation was also sampled in this drill core. Ten samples were collected from this formation encompassing a vertical thickness of 7.1 m. Samples were oriented by the lamination dip directions. SInce the same mean dip was measured for the Cerro Negro and Avellaneda Formations, the same bedding attitude determined for the latter was used for the Cerro Negro samples (Strike Az: 20°, dip: 17°). Demagnetization of the specimens proceeded following the same scheme applied to samples from the Avellaneda Formation. Only high

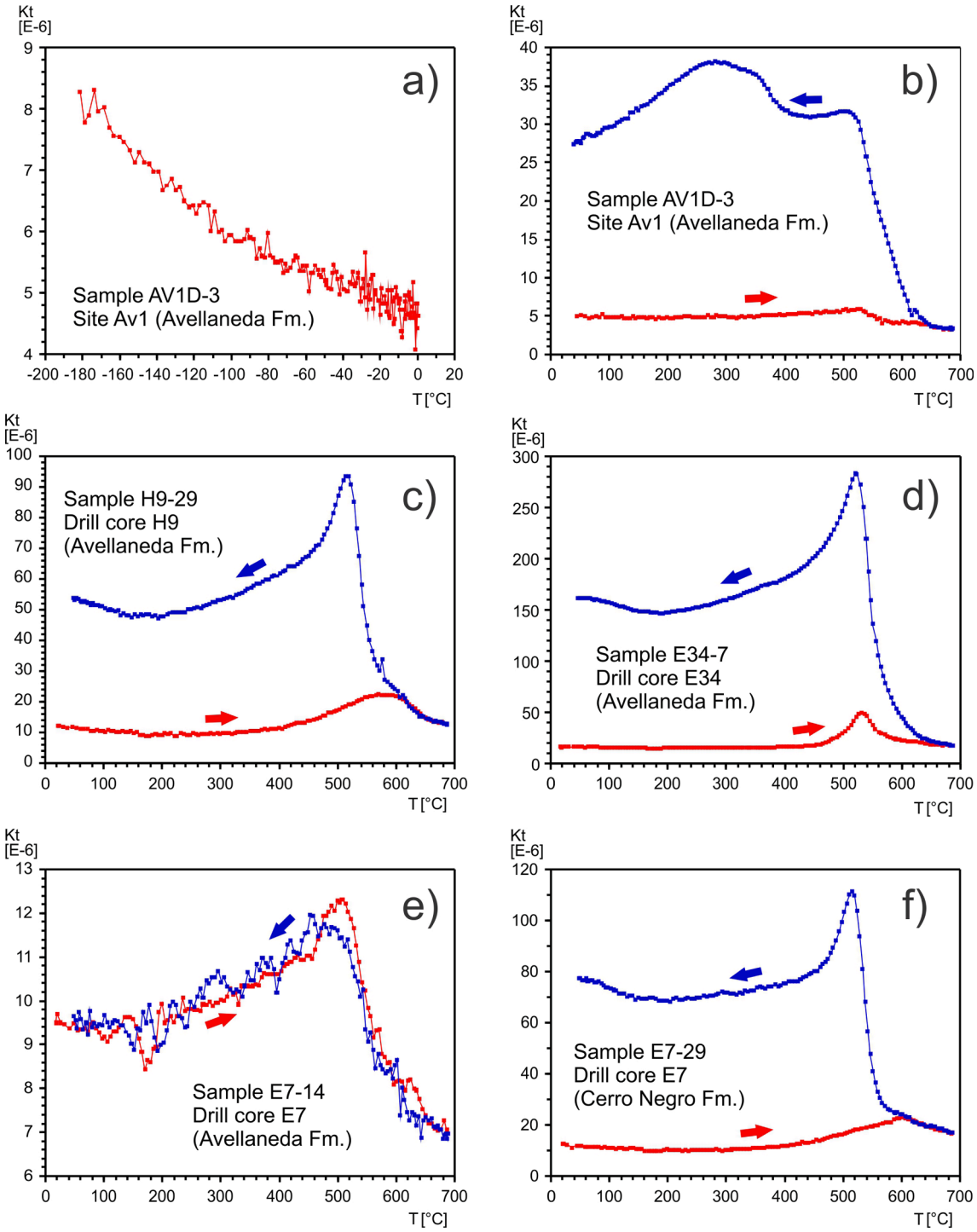

Fig. 12. Low and high temperature thermomagnetic curves. a) Normalized low temperature curve for a sample of the Avellaneda Formation from site AV-1 (outcrop); b) high temperature curves for the same sample; c), d) and e) high temperature curves from samples of the Avellaneda Formation from H9; E34 and E7 drill cores, respectively; f) high temperature curves for a sample from the Cerro Negro Formation, taken from drill core E7. The red (blue) lines correspond to the heating (cooling) curves. Most samples generally show irreversible curves with possibly neo formation of magnetite. (For interpretation of the references to color in this figure legend, the reader is referred to the web version of this article.)

Table 5
Coercitive force (Bc) and remanence coercivity (Bcr) values for samples of the Avellaneda Formation in drill cores E34, E7 and H9 and site AV1. The values obtained for the Cerro Negro Formation in the drill core E7 are also shown. Note that there is not a clear correlation between lithology and the values obtained. Bc and Bcr in mT.

Drill core (formation)	Lithology	Core	Bc	Bcr
E34 (Avellaneda Formation)	marl	E34-1	44.6	74.8
	marl	E34-2	29.1	56.1
	marl	E34-3	70.4	290.8
	marl	E34-4	37.0	85.5
	marl	E34-5	316.0	422.8
	marl	E34-6	308.0	434.9
	marl	E34-7	312.2	414.6
	shale	E34-8	187.6	385.7
	shale	E34-9	370.5	433.7
	marl	E34-10	100.9	359.8
	shale	E34-11	180.7	364.7
	marl	E34-12	94.3	298.7
E7 (Avellaneda Formation)	marl	E7-22	361.8	456.1
	marl	E7-26	348.2	439.3
	marl	E7-37	21.2	47.1
	marl	E7-40	33.9	84.8
H9 (Avellaneda Formation)	marl	H9-9	52.7	242.9
	marl	H9-18	78.7	351.4
	marl	H9-21	297.5	404.6
	shale	H9-26	361.0	452.6
AV1 (Avellaneda Formation)	shale	AV1A-1C	–	469.9
	shale	AV1A-4B	–	467.5
	shale	AV1D-3	41.7	108.2
	shale	AV1E-4B	–	395.7
E7 (Cerro Negro Formation)	shale	E7-29	305.7	403.9
	sandstone	E7-32	51.0	307.2
	shale	E7-35	277.8	360.3

temperature demagnetization with steps like those described above for the Avellaneda Formation was applied. A low temperature component "A" was isolated between 90 and 300°/350 °C. The mean direction of component "A" isolated was virtually identical to that from the Avellaneda Formation in this drill core confirming the validity of the same bedding correction. Component "B" was isolated between 350 and 575° C, although in some occasions unblocking temperatures above 600° C were found (Fig. 8a). With a single exception, all specimens carried a NNW downward directed component "B" with moderate to high Inclinations. The mean direction obtained for component "A" "in situ" was: Dec: 4.9°; Inc: −30.0°; α_{95}: 5.1°; k: 39.8; n: 21 and after bedding correction: Dec: 356.6°; Inc: −24.3°; α_{95}: 5.1°; k; 39.8. The Inclination only mean yielded a value of Inc: −29.7°, α_{95}: 4.8°, k: 30.7, n: 21 in geographic coordinates and values of Inc: −24.1°, α_{95}: 4.9°, k: 30.2 after bedding correction. The mean "in situ" direction obtained from component "B" is n: 31, Dec: 347.8°, Inc: 58.8°, α_{95}: 5.9°, k: 20.3, while after bedding correction the mean direction is: Dec: 18.2°, Inc: 64.0°, α_{95}: 5.9°, k: 20.3 (Fig. 8b, Table 2 and 4).

Like in Avellaneda Formation (drill hole E7), a great circle analysis was performed for all specimens of the Cerro Negro Formation. In geographic coordinates, at specimen level, a great circle intersection was determined at Dec: 325.7°, Inc: 67.3°, α_{95}: 5.1° (Table 3), while the mean direction computed from PCA analysis is Dec: 347.8°, Inc: 58.8°, α_{95}: 5.9°, n: 31. After bedding correction, the great circle intersection is at Dec: 12.4°, Inc: 76.8° (Table 3) and the mean direction from PCA computation is Dec: 18.2°, Inc: 64.0°. It is clear that a significantly steeper remanence direction is inferred from the great circle intersection analysis and that some contamination of component "A" on "B" is likely. Also, the analysis was made by the mean great circle intersection for each sample. In geographic coordinates, the great circle intersection is Dec: 333.4° Inc: 66.0°, α_{95}: 12.4° (Table 3) while the PCA mean direction is Dec: 348.3°, Inc: 58.7°, α_{95}: 10°, N: 10. After bedding correction, the great circle intersection is at Dec: 16.9°, Inc: 73.8° and the PCA mean direction is Dec: 18.5°, Inc: 63.7°. This confirms the results obtained from the analysis made on a specimen basis suggesting some unerased overlap between components "A" and "B" (Table 3 and Fig. 10).

5. Directional analysis

5.1. Mean directions determined on a specimen basis

From the study carried out at the outcrop level at site AV1 and in drill cores E34, H9 and E7, a mean direction for the ChRM can be obtained considering all specimens for the Avellaneda Formation. This yields an "in situ" direction (after azimuthal orientation) of: Dec: 6.6°, Inc: 59.3°, α_{95}: 2.4°, k: 15.1, n: 246. After application of the respective bedding corrections an improvement in the statistical parameters is observed: Dec: 18.6°, Inc: 65.1°, α_{95}: 2.2°, k: 18.3 (Fig. 9).

5.2. Mean direction determined on a sample basis

The mean direction for the Avellaneda Formation was also determined by averaging the specimen ChRM directions per core segment in order to obtain a single direction for each independent sample of the drill cores and the outcrop. In this way, each sample (approximately 10 to 30 cm long segments of the cores) resembles a more traditional paleomagnetic site. This procedure was carried out either considering all samples regardless of the number of specimens contributing to each mean or selecting only those samples with a number of specimens ≥ 3 (Fig. 10a, Fig. 11). The mean direction obtained considering all samples in "in situ" geographic coordinates is: Dec: 6.5°, Inc: 59.1°, α_{95}: 4.2°, k: 17.3, N: 69, and after applying the bedding correction the statistical parameters improve slightly: Dec: 18.8°, Inc: 64.2°, α_{95}: 3.8°, k: 20.8. This improvement is not significant at 95 % confidence. On the other hand, the mean direction from samples with three or more specimens in "in situ" geographic coordinates is: Dec: 7.0°, Inc: 60.9°, α_{95}: 4.8°, k: 18.3, N: 51 and when applying the bedding correction is: Dec: 21.4°, Inc: 67.0°, α_{95}: 4.1°, k: 24.2, again showing a slight improvement in the statistical parameters after bedding correction. Application of the McElhinny (1964) tilt test turns a significant pre-tilt magnetization at

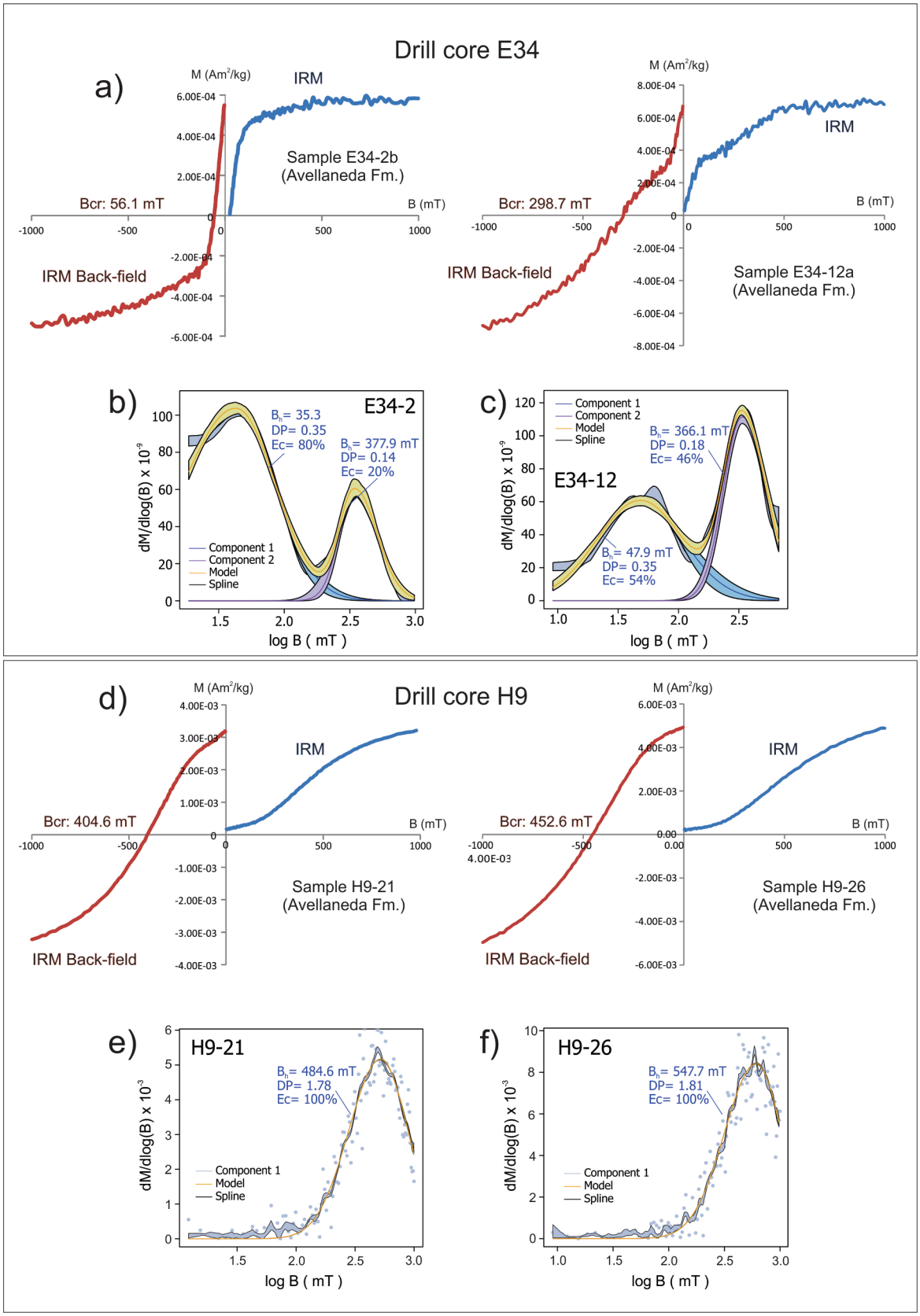

Fig. 13. Isothermal remanent magnetization (IRM) and IRM back-field acquisition curves, a) Curves belonging to representative samples of the Avellaneda Formation from drill core E34; b) and c) MAXunMix modeling from IRM data showing coercivity component from the previous samples; d) idem a) for representative samples from drill core H9; e) and f) idem b) and c) for the samples of the drill core H9. Bcr: coercivity of remanence.

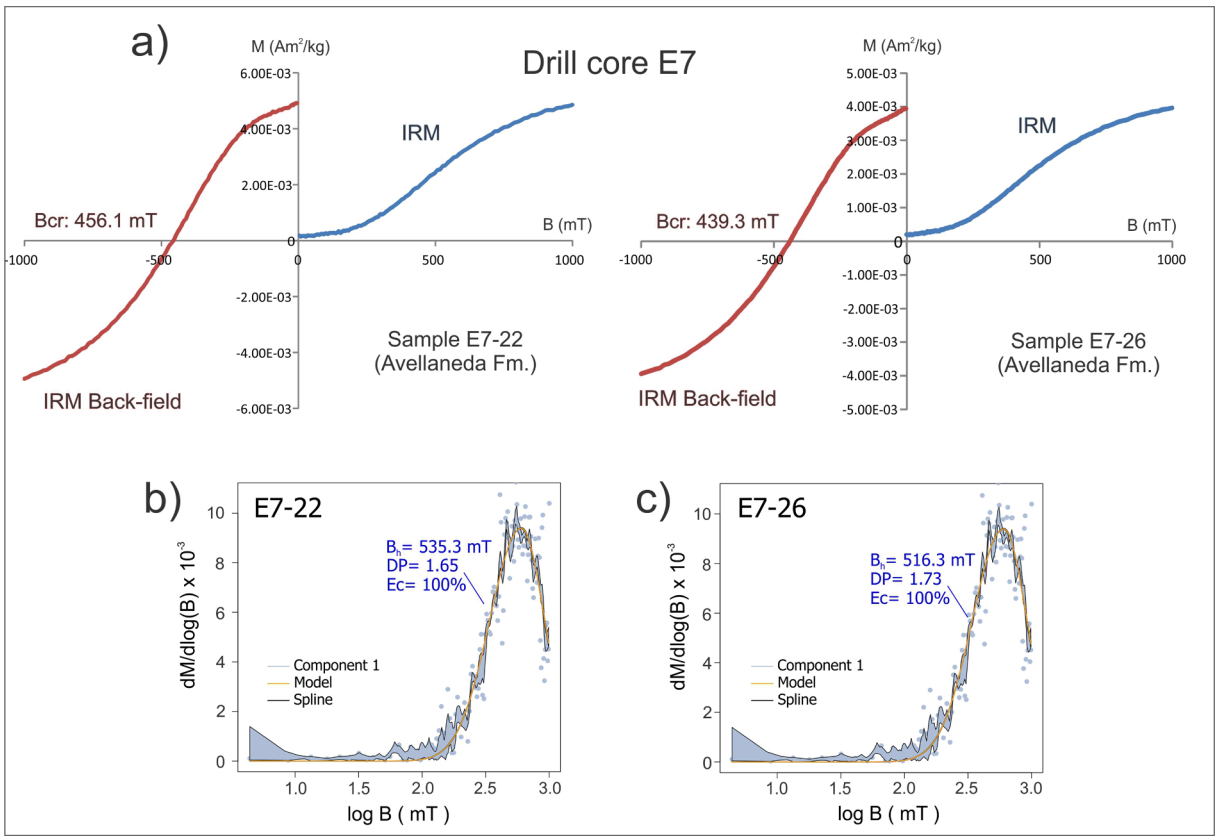

Fig. 14. Isothermal remanent magnetization (IRM) and IRM back-field acquisition curves, a) Curves belonging to representative samples of the Avellaneda Formation from drill core E7; b) and c) MAXunMix modeling from IRM data showing coercivity component from the previous samples. Bcr: coercivity of remanence.

90 % but not-significant at 95 %. In any case, the results suggest that a pre-tilting remanence is more likely. Regarding the folding age, Hernández et al. (2017) estimated an Ediacaran age for the deformation, that could have lasted until Cambrian times according to structural studies carried out by Massabie and Nestiero (2005). As shown in Table 4, the method for determining the mean direction of the Avellaneda Formation, whether by averaging all specimens, all samples or only samples with a number of specimens equal or greater than 3, does not yield significantly different results.

In the Cerro Negro Formation, an analysis was also carried out to determine the mean direction on a sample (and not specimen) basis. In this case, due to the low number of samples, no selection was made based on the number of specimens. A complete directional analysis was made considering the mean directions of the samples obtained in this work and those directions reported by Rapalini et al. (2013) for the same formation (see Table 2). The mean direction for the Cerro Negro Formation computed in this way is Dec: 353.9°, Inc: 57.9°, α_{95}: 8.5°, k: 23.0, N: 14. When applying the bedding correction the mean direction is Dec: 19.8°, Inc: 60.7°, α_{95}: 7.7°, k: 27.7, observing a slight improvement in the statistical parameters but not statistically significant (Fig. 10b). However, Rapalini et al. (2013) reported a positive fold test for this formation.

On the other hand, a great circle analysis was carried out in all of the Cerro Negro specimens here reported. The great circles intersections obtained are shown in Table 3 and Fig. 10c. If we compare the directions determined with principal component analysis for Cerro Negro Formation (see Table 2 and 4) and those determined with great circle analysis, a significant difference (~9°, see Table 3) is evident, suggesting that contamination of ChRM directions by unerased contributions from the A component is likely. Therefore mean site ChRM were in this case computed by great circle analysis (McFadden and McElhinny, 1988).

5.3. Reversal tests

The paleomagnetic records of the Avellaneda Formation suggest a dominant reverse polarity with some short periods of normal polarity (see below and Afonso et al., 2022 companion paper). A reversal test was applied to the Avellaneda Formation ChRM directions after bedding correction (McFadden and McElhinny, 1990, Koymans et al., 2016). In two cores the reversal test yielded negative results (E34, angle between directions of 12.3° vs critical angle of 8.3°, E7, angle between directions of 29.0° vs critical angle of 6.7°). At core H9 the result was classified as indeterminate, with an angle between directions of 12.3° and a critical angle of 31.2°. When the reversal test was determined for all specimens (n: 246), both in geographic coordinates and after bedding correction, the result was still negative. In geographic coordinates, the angle between directions was 22.9° vs critical angle 7.8°, meanwhile after bedding correction the angle between directions was 23.9° vs critical angle 6.3°. Failure of the reversal test may indicate that the sampling of normal intervals was not sufficient to fully average the paleosecular variation or an incomplete desmagnetization of the component "A". In this sense, a new reversal test was carried out considering the great circle intersection directions from the reverse and normal polarities specimens in drill core E7. The directions obtained are shown in Table 3. In this case, the reversal test is still negative, with an angle between directions of 10.4° and a critical angle of 9.2°. As can be seeing in Fig. 7, the analysis of great circles allows to reduce the angular difference but the test still fails.

6. Rock magnetism

Rock magnetism studies were carried out in representative samples from the three drill cores and from the outcrop of the Avellaneda and Cerro Negro Formations. The studies consisted of K (bulk susceptibility)

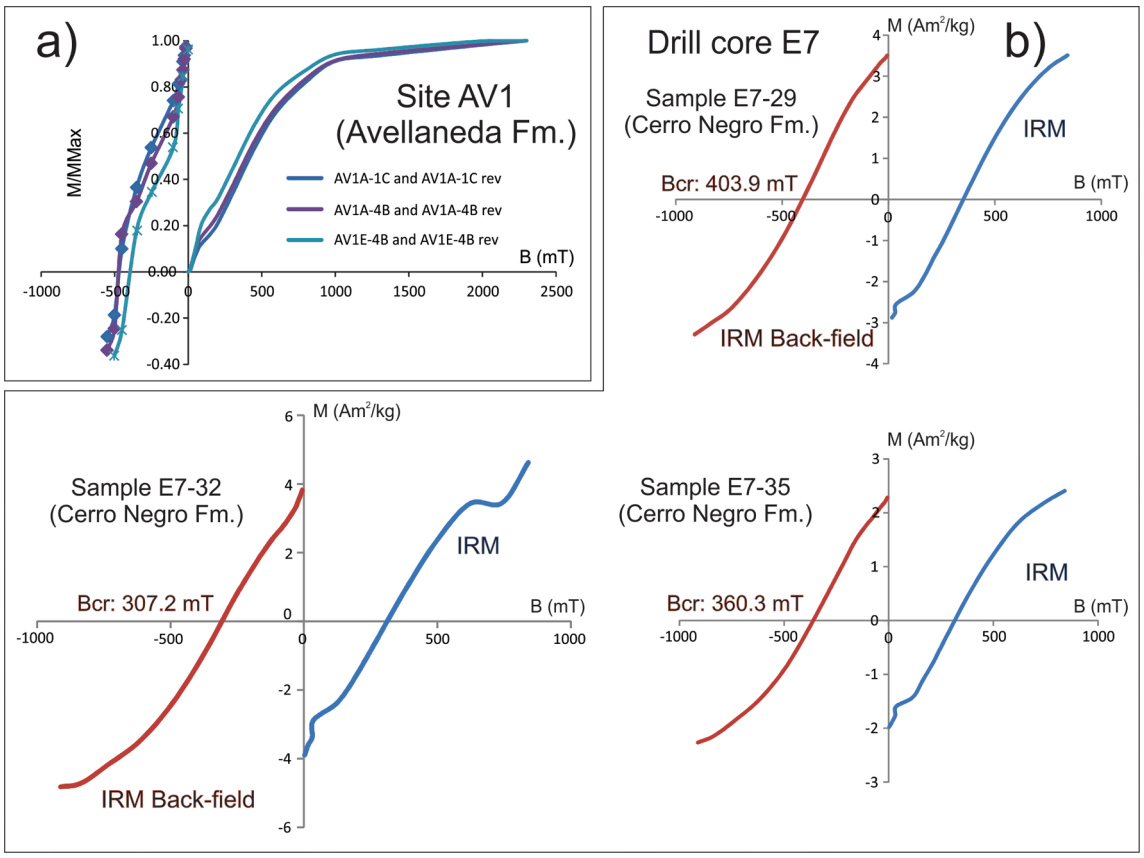

Fig. 15. Isothermal remanent magnetization (IRM) and back-field acquisition curves, a) Curve belonging to the Avellaneda Formation at site AV1; b) Curves belonging to representative samples of the Cerro Negro Formation from drill core E7. Bcr: coercivity of remanence.

vs T, IRM (isothermal remanent magnetization) acquisition and back-field curves, hysteresis cycles and FORCs diagrams.

6.1. *Thermomagnetic curves*

The K vs T curves were performed at low and high temperatures in the AV1D-3 sample (marl) taken from the AV1 site (Avellaneda Formation). The low temperature susceptibility curve (Fig. 12a) shows the typical behavior of paramagnetic minerals as mainly responsible for susceptibility. On the other hand, the high temperature curve (Fig. 12b), carried out under argon atmosphere, shows a minor drop in K between 540 °C and 580 °C, consistent with the presence of magnetite. Cooling curve shows an irreversible cycle indicating mineralogical changes in response to heating. The peaks in susceptibility observed in the high temperature cooling curve indicate the formation of new ferromagnetic (*sensu lato*) phases (magnetite?, maghemite?) as a product of the alteration during heating. The same happens in the high temperature curves from samples of the Avellaneda Formation in H9 (sample H9-29, shale) and E34 (sample E34-7, marl) drill cores (Fig. 12c, d). In these latter cases, production of magnetite seems obvious due to the steep increase in susceptibility with cooling just below 580 °C. In all these cases a five to ten fold increase in K at room temperature is observed after heating. A different behavior is observed in the sample E7-14 (marl) taken from the Avellaneda Formation in drill core E7 (Fig. 12e), with a noisy but basically reversible cycle. During heating an apparent Hopinson peak (Dunlop and Özdemir, 1997) develops followed by a steep delay in K around 540–580 °C compatible with (Ti poor) magnetite. Finally, the sample E7-29 (sandstone) from the Cerro Negro Formation (drill core E7) presents a behavior similar to that of most of the samples analyzed in the Avellaneda Formation, with irreversible cycle and neo formation of magnetite producing a fivefold increase in K at room temperature (Fig. 12f).

6.2. *IRM and IRM back-field*

The IRM and IRM back-field curves were performed on 12 specimens from the Avellaneda Formation, at E34, four specimens from H9 and E7, each, and one specimen from AV1 (Table 5). Three specimens of the Cerro Negro Formation collected from E7 drill core were also analyzed. The samples from the drill core E34 showed mostly behaviors associated to ferrimagnetic minerals, reaching saturation at fields lower than 1 T and a steep increase in the curve at low fields (Fig. 13a, sample E34-2b, marl). The exception was the sample E34-10, at the upper part of the section, where hematite is dominant. In most cases, where ferrimagnetic minerals are dominant, there is clear evidence of an additional antiferromagnetic contribution (Fig. 13a, sample E34-12a, marl). The remanence coercivity (Bcr) yielded a wide range of values, between 56.1 and 434.9 mT. As can be seen in Table 5, low Bcr values are observed in the lower stratigraphic levels (samples E34-1 and E34-2) while in the upper levels, values of a higher order of magnitude are consolidated, with a more stratigraphic correlation prevailing than lithological with the value of Bcr. Statistical unmixing of different phases contributions was achieved using MAXunMix application (Maxbauer et al., 2016 and references therein). The result for some selected samples is presented in Fig. 13 b and c for drill core samples E34. The qualitative interpretation just described is confirmed by this analysis. Both samples show the presence of two components with significantly different coercive forces (Bc) likely corresponding to magnetite (41–39 mT) and hematite (620–477 mT), respectively, with medium to strong predominance of hematite. However, the presence of maghemite as a remanence carrier must be considered likely as a high coercive force phase. This is consistent with the amplitude of unblocking temperatures observed in

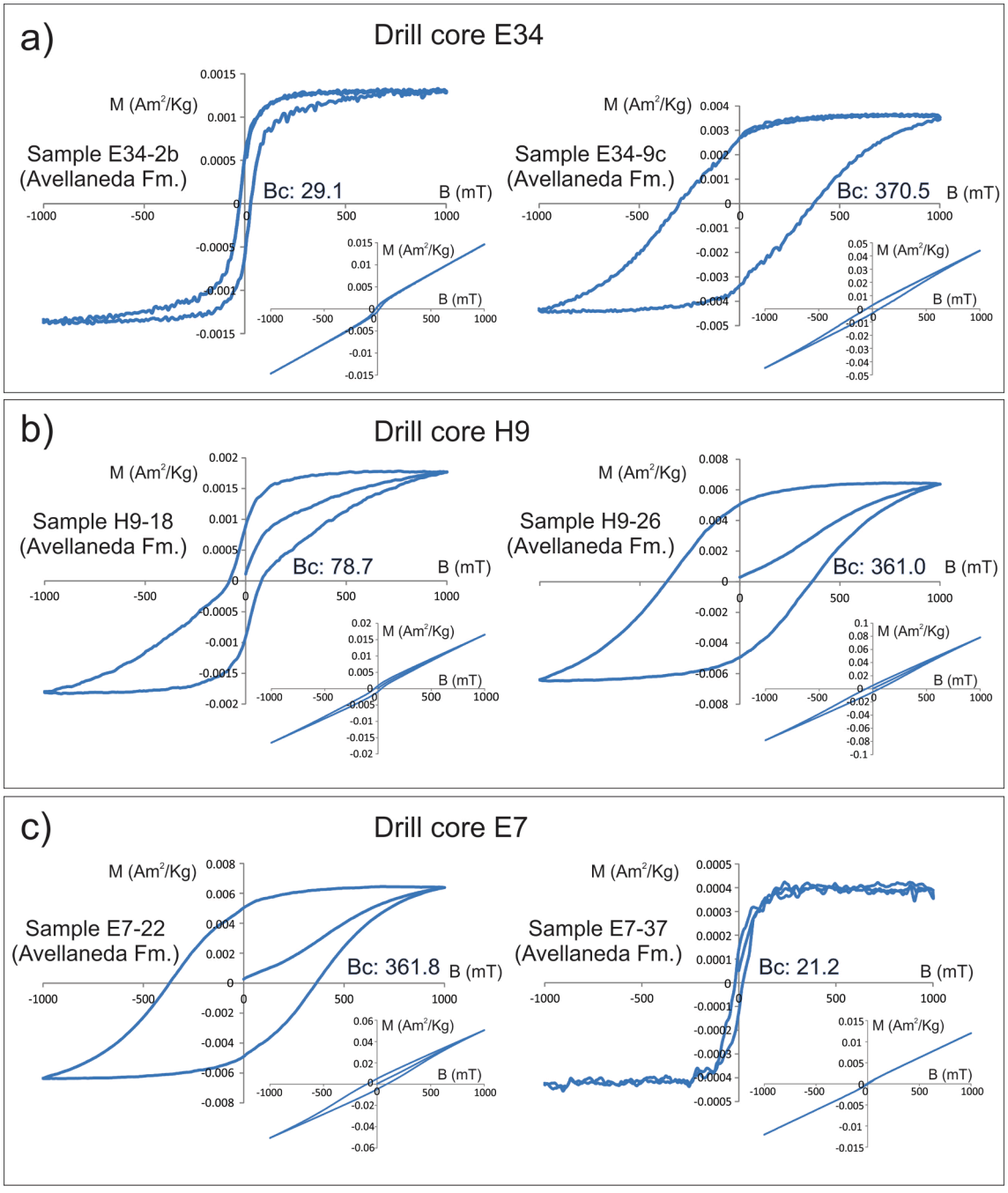

Fig. 16. a) Representative hysteresis cycles of the Avellaneda Formation in drill core E34; b) and c) idem a) for drill cores H9 and E7, respectively, after subtraction of the paramagnetic contribution. In the insets, the original "uncorrected" cycles are shown. Bc: coercive force in mT.

the demagnetization diagrams (Fig. 5a).

In drill core H9, a behavior opposite to the previous drill core is observed (Fig. 13d) with a predominance of the antiferromagnetic fraction, easily identifiable from the less abrupt increase in magnetization at low fields and from non-saturation at smaller fields than 1 T. This behavior is observed in rocks of different lithology, being the samples H9-9, H9-18 and H9-21 marls, and H9-26 a shale sample. The remanence coercivity values obtained were similar to each other, between 242.9 and 452.6 mT (Table 5). The analyses using the MAXunMix application are consistent results with the IRM method, based on the predominance of an antiferromagnetic component (Fig. 13e, f).

As in the previous case, drill core E7 showed antiferromagnetic fraction in samples E7-22 and E7-26 located in the upper section of the stratigraphic column (Fig. 2 and Fig. 14) but a ferrimagnetic fraction was observed in the other two samples located in the lower part (E7-37 and E7-40, Fig. 2 and Table 5). In both cases, the lithology remains the same with the presence of marls. The remanence coercivity varied between 47.1 and 456.1 mT (Table 5). Finally, at the AV1 site, a marked predominance of the antiferromagnetic fraction is seen (Fig. 15a), with remanence coercivity values between 108.2 and 469.9 mT (Table 5). It is

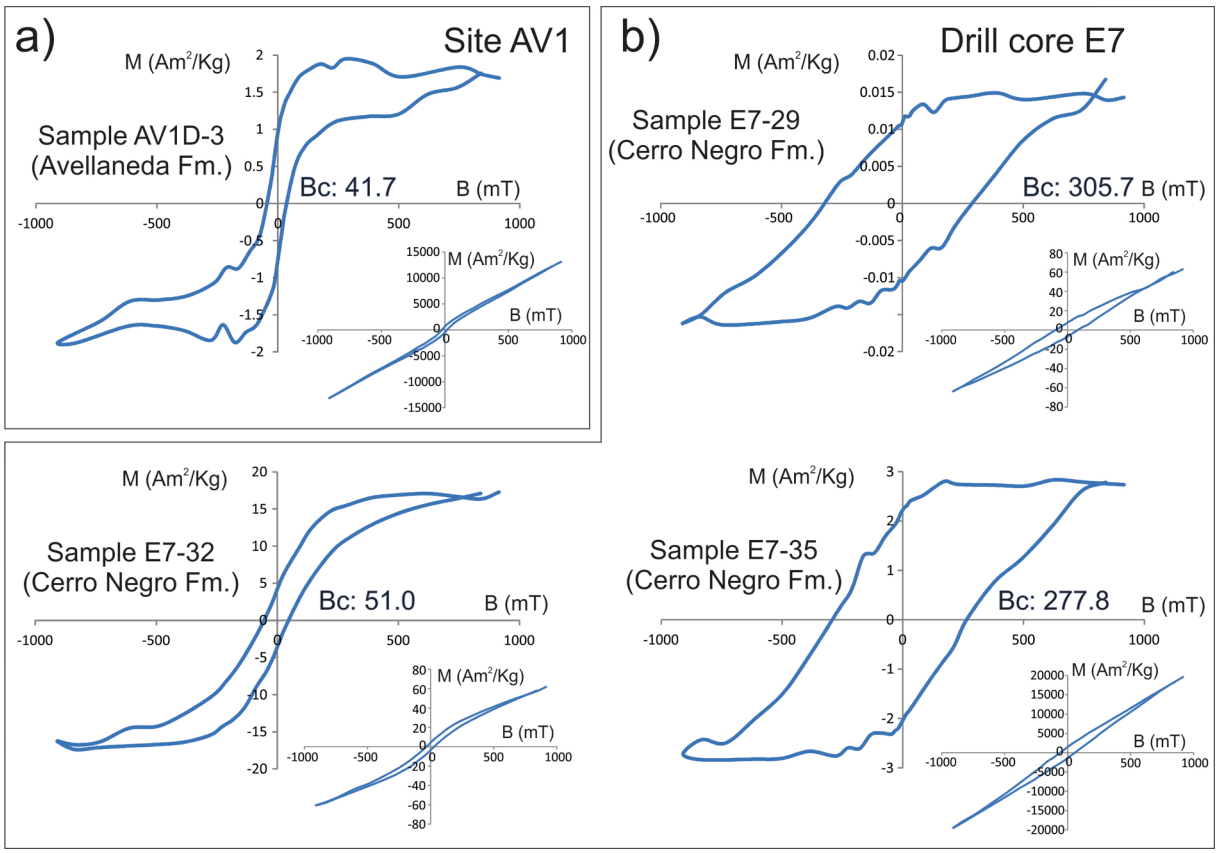

Fig. 17. a) Representative hysteresis cycle of the Avellaneda Formation at the AV1 site; b) representative hysteresis curves of the Cerro Negro Formation in drill core E7. References as in Fig. 16.

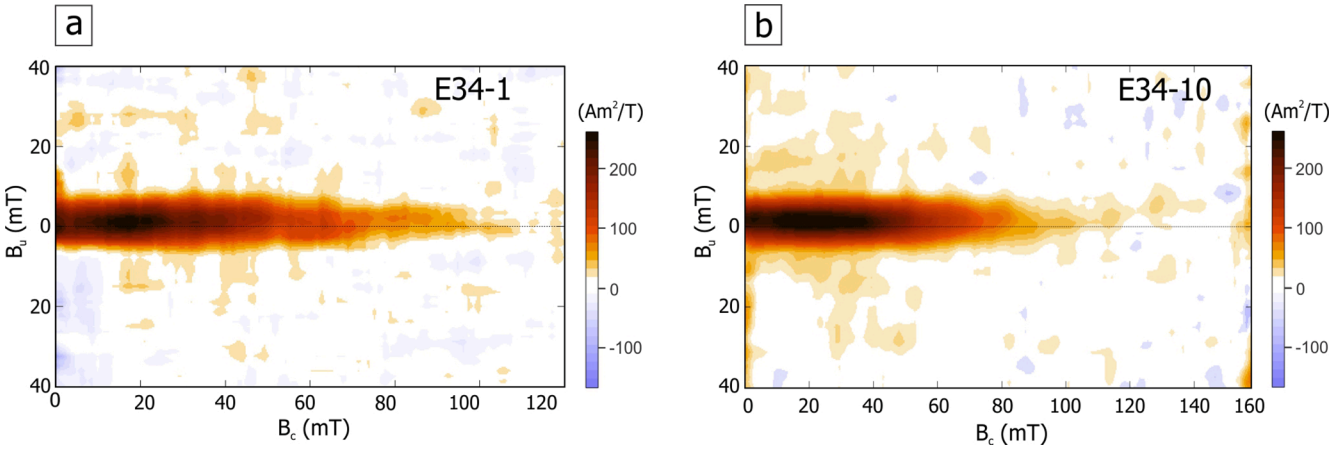

Fig. 18. FORCs diagrams from the E34-1 and E34-10 samples.

important to mention that the determination of IRM and IRM back-field in this case was carried out by an ASC Scientific IM-10–30 pulse magnetizer applying the following steps to IRM: 15, 29, 44, 61, 74, 100, 150, 200, 300, 450, 600, 800, 1000, 1310, 1970 and 2300 mT. On the other hand, the pulses applied for the IRM back-field were: 15, 25, 35, 65, 100, 250, 350, 450, 500 and 550 mT. The study of the AV1D-3 sample (not shown in Fig. 15) was carried out using a VSM magnetometer (Molspin ltd.).

In the Cerro Negro Formation, there is a clear predominance of the antiferromagnetic fraction (Fig. 15b). The IRM back-field curves yielded remanence coercivity values between 307.2 and 403.9 mT (Table 5).

6.3. *Hysteresis cycles*

The hysteresis cycles, performed on the same IRM samples, showed an important contribution of paramagnetic minerals (Figs. 16 and 17), in all the analyzed samples and in the two formations studied. After subtracting the paramagnetic contribution, moderate to high coercive forces were observed in the Avellaneda Formation, with a wide range of values between 29.1 and 370 mT in drill core E34, between 52.7 and 297.5 mT in drill core H9, and between 21.2 and 361.8 mT in drill core E7 (see Table 5). Finally, a single hysteresis cycle was performed at the AV1 site, obtaining a moderate coercivity Bc: 41.7 mT. In the Cerro Negro Formation, the coercivity values were also moderate to high

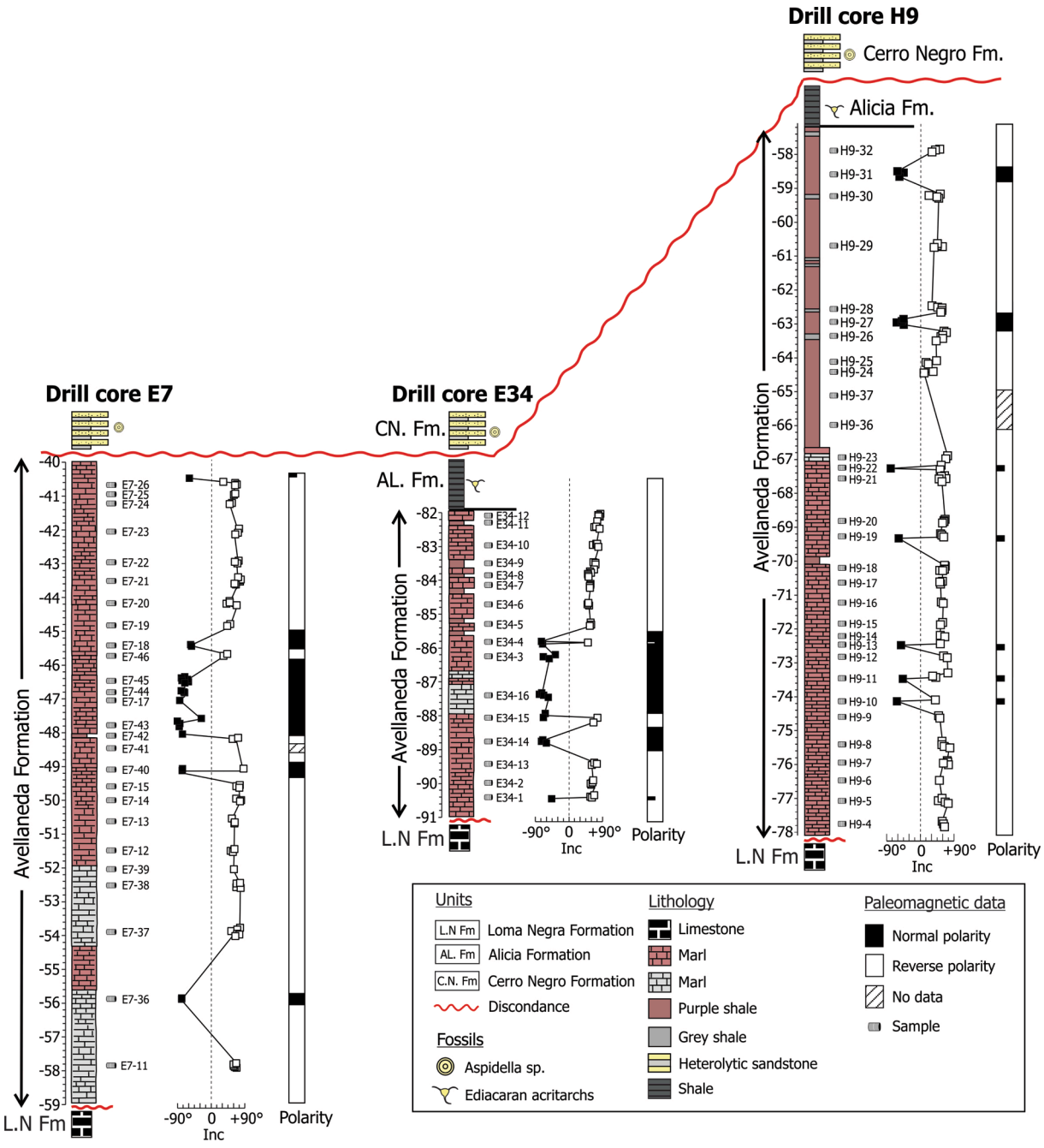

Fig. 19. Magnetostratigraphic columns obtained for the Avellaneda Formation at drill cores E7, E34 and H9. For a detailed discussion of the magnetostratigraphic results and their implications, see the companion paper by Afonso et al. (2022). Modified from Afonso et al. (2022).

(between 51.0 and 411.0 mT, Table 5) with a slightly higher mean value (Bc mean: 211.5 mT). From Figs. 16 and 17, it is possible to observe a significant disparity in the shapes of the hysteresis curves within each drill core and in both formations. This is analyzed based on the stratigraphic height and by comparison with the IRM and thermomagnetic curves. In drill core E34, hysteresis curves show "pseudo-single domain" loops (sample E34-2b, Fig. 16a), shapes determined by the presence of hematite (sample E34-9c, Fig. 16a) and "goose-neck" loops, following the classification proposed by Tauxe (2005). These curves are coherent with the behaviors observed in the IRM curves (Fig. 13a) where a predominance of magnetite was observed (80–54 %) with a subordinate antiferromagnetic (hematite) fraction (20–46 %). In drill core H9, hysteresis curves showed "goose-neck" loops (sample H9-18, Fig. 16b) and shapes determined by the presence of hematite (sample H9-26, Fig. 16b), which is corroborated with the coercivity spectra (Fig. 13f). Finally, the drill core E7 has hysteresis curves with shapes determined by the presence of hematite (sample E7-22, Fig. 16c) and "pseudo-single domain" loops (sample E7-37, Fig. 16c). Stratigraphic height does not show a clear correlation with magnetic mineralogy (Table 5, Fig. 2). In the drill cores E34 and E7 the predominance of marls is almost absolute, with shaly levels near the top of the Avellaneda Formation. In the case of the former, the predominance of magnetite does not change with

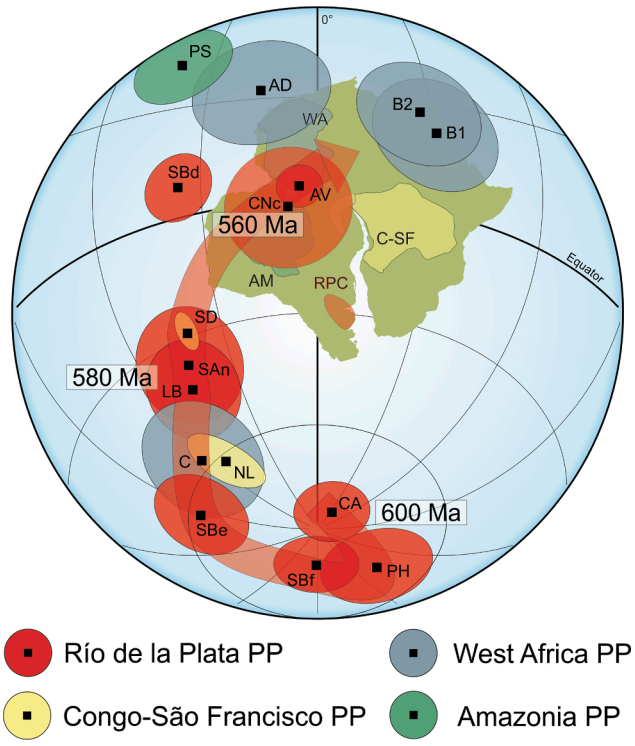

Fig. 20. Proposed APWP for the RPC in the 600–550 Ma interval. The paleomagnetic poles of other Western Gondwana cratons for the same interval are also shown. The RPC and Congo-São Francisco poles were rotated to Africa according to the Euler pole 47.5° N, 33.3° W, 56.2° ccw (Torsvik et al., 2012), while the Amazonia pole was rotated according to 50° N, 32.5° W, 55.1° ccw (Torsvik et al., 2012). For the acronyms used in the poles see Table 6. The white boxes next to the APWP indicate approximate ages in that section.

lithology (marl or mudstone), being the exception sample E34-10 (predominance of hematite in marl). In the second, the analyzed samples that are in the upper levels (E7-22 and E7-26) show a predominance of hematite while for the samples analyzed in lower levels (E7-37 and E7-40) a predominance of magnetite is inferred. Finally, in drill core H9, a greater contribution of detrital material is observed in the upper part of the Avellaneda Formation between 63.5 and 58 m (below surface), approximately. All samples showed a predominance of hematite, irrespective of them belonging to marls or to shales (sample H9-26). The Cerro Negro Formation, only represented in drill core E7, shows hysteresis curves with shapes determined by the presence of hematite (sample E7-29 and E7-35, Fig. 17b) and "pseudo-single domain" loops (sample E7-32, Fig. 17b). The IRM curves show the presence of antiferromagnetic minerals (Fig. 15b) and the high temperature thermomagnetic curve is consistent with the presence of hematite and magnetite (Fig. 12f).

Table 6
Ediacaran poles belonging to the Río de la Plata, Congo-São Francisco, West Africa and Amazonia cratons. They are reported in current coordinates and in Gondwana coordinates. The rotations of the paleomagnetic poles were made according to the Euler poles (Torsvik et al., 2012): RPC (47.5°N, 33.3°W, 56.2° ccw) and Amazonia (50.0°N, 32.5°W, 55.1° ccw). Pole references: 1- This paper; 2- Rapalini et al. (2013); 3- Rapalini (2006); 4- Rapalini et al. (2015); 5- D'Agrella Filho and Pacca (1988); 6- Meert and Van der Voo (1996); 7- Moloto-A-Kenguemba et al. (2008); 8- Morel (1981); 9- Robert et al. (2017); 10- García et al. (2013). Lat: latitude, Long: longitude. GCA: Cerro Negro Formation pole computed with great circle analysis plus samples reported by Rapalini et al. (2013). PCA: Cerro Negro Formation pole computed with principal component analysis plus samples reported by Rapalini et al. (2013).

			Present-day coordinates		Pole position (Gondwana coordinates)				
Craton	Geologic unit	Pole	Lat (°)	Long (°)	Lat (°)	Long (°)	A_{95} (°)	Age (method)	Ref.
Río de la Plata	Cerro Negro (GCA)	CNc	−3.6	307.8	−1.3	352.4	16.6	558–550 (APWP and paleontology)	1
	Cerro Negro Fm. (PCA)	CN	7.0	314.4	11.2	351.3	9.5	558–550 (APWP and paleontology)	1
	Avellaneda Fm.	AV	−1.0	313.4	4.1	355.3	5.9	570 (APWP and stratigraphy)	1
	Olavarría Fm.	SBd	21.0	290.4	8.2	323.9	8.9	560 (APWP)	2
	Los Barrientos	LB	−16.2	253.9	−42.4	312.6	12.9	570 (APWP)	3
	Sierra de Animas Complex	SAn	−12.2	258.9	−36.5	315.3	14.9	578 ± 4 (U-Pb SHRIMP, zircon)	4
	Cerro Largo Fm.	SBe	−25.9	219.0	−62.9	265.7	11.3	580 (APWP)	2
	Villa Mónica Fm.	SBf	−49.0	198.2	−78.6	181.4	9.2	590 (APWP)	2
	Playa Hermosa Fm.	PH	−58.8	183.1	−71.2	137.1	12.1	590 (U-Pb SHRIMP, detrital zircons)	4
	Campo Alegre Fm.	CA	−57.0	223.0	−83.9	33.9	9.0	600 (APWP)	5
Congo-São Francisco	Sinyai Dolerite	SD	−29.0	319.0	–	–	3/5	547 ± 4 (Ar-Ar, biotite)	6
	Nola Dyke	NL	−61.8	304.8	–	–	5.4/10.7	571 ± 6 (Ar-Ar, amphibole)	7
West Africa	Adma Diorite	AD	32.5	344.7	–	–	15.9	616 ± 11 (U-Pb, zircon)	8
	Fajjoud and Tadoughast Volc.	B1	21.9	31.0	–	–	15.6	572–551 (U-Pb SHRIMP, zircon)	9
	Djebel Boho Volc.	B2	27.3	27.1	–	–	14.9	547–526 (U-Pb SHRIMP, zircon)	9
	Adrar-*n*-Takoucht Volc.	C	−57.6	295.6	–	–	15.7	577–564 (U-Pb SHRIMP, zircon)	9
Amazonia	Planalto da Serra	PS	49.7	313.4	42.6	319.8	10.8	615 ± 5 (Ar-Ar, phlogopite)	10

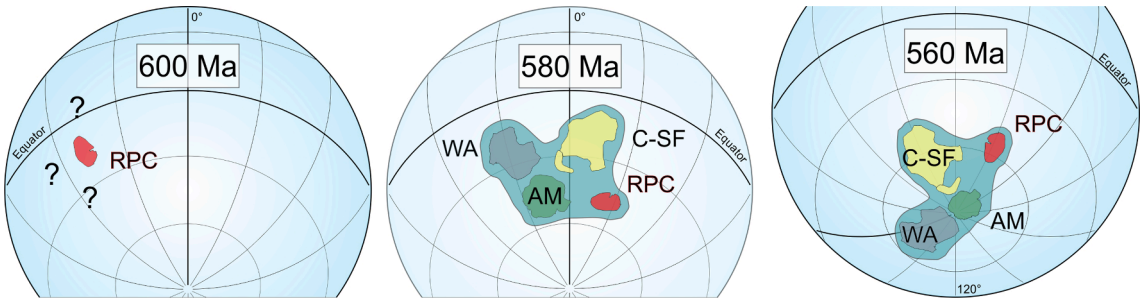

Fig. 21. Paleogeography of the RPC at 600, 580 and 560 Ma. At 600 Ma there is no paleomagnetic evidence that supports the RPC together with another Gondwana craton. From ~ 575 Ma, paleomagnetic information allows more complete paleoreconstructions. WA: West Africa; AM: Amazonia; C-SF: Congo-São Francisco.

6.4. First-order reversal curve (FORC) analyses

FORC studies were carried out in six samples from E7 (E7-37 and E7-40), H9 (H9-9 and H9-21) and E34 (E34-1 and E34-10) drill cores providing more details about the magnetic remanence in the Avellaneda Formation. All representative samples show a highly peaked line on the $B_u = 0$ axis with contours elongated across Bc axis. The presence of a lobe extending along the negative B_u axis (Fig. 18) is characteristic of interacting SD magnetite. Similar distributions have been observed for experimentally disaggregated magnetosome particles (Kopp and Kirschvink, 2008; Moskowitz et al., 1993) and for some magnetofossil-bearing sediments (Egli et al., 2010; Roberts et al., 2011, 2012; Yuan et al., 2019). The sample E34-12 show a broader vertical spread close to the origin of the Bc axis indicating some contributions of super-paramagnetic fractions (Roberts et al., 2014).

7. Discussion

Our study of the Ediacaran Avellaneda and Cerro Negro Formations allowed us to compute two new paleomagnetic poles for the Río de la Plata Craton. The directional analysis of the Avellaneda Formation was carried out with two methodologies: by averaging the specimens and by considering the mean directions obtained in each sample. From this last methodology, mean directions were determined from samples with $n \geq 3$ specimens and without such restriction. In the case of the Cerro Negro Formation, the directional analysis was performed in the same way but without applying any restriction to the number of specimens per sample. In the latter, we resorted to the analysis of remagnetization circles to better define the ChRM. As seen in Table 4, the final mean directions obtained either by averaging specimens or samples do not vary significantly. In the two studied formations, the specimen directions and mean directions per sample were converted into VGPs in order to compute the respective paleomagnetic poles. In all three drill cores analyzed dominant reverse polarity is ubiquitous. However, some short intervals of opposite polarities have been found (Fig. 19). For a detailed discussion on the magnetostratigraphy of the Avellaneda Formation the reader is referred to the companion paper of Afonso et al. (2022). No reversals were observed in the outcrop sampled at AV1, however such small sampling only encompassed 6 m of stratigraphic thickness. The Cerro Negro Formation exhibits a similar behavior to the underlying Avellaneda Formation, with a large predominance of specimens with reverse polarity (a single specimen showed normal polarity).

The paleomagnetic poles determined for the Avellaneda (1.0°S, 313.4° W, A_{95}: 5.9°) and the Cerro Negro (3.6° S, 307.8° E, A_{95}: 16.6) Formations are located close to each other. They are presented in Fig. 20 in West Africa coordinates in a Western Gondwana reconstruction (Torsvik et al, 2012), and in Table 6, together with other Ediacaran poles from Western Gondwana cratons (i.e. Río de la Plata, Amazonia, West Africa and Congo-São Francisco). As has been already published several times (see Rapalini, 2018) a simple and long apparent polar wander path seems to accommodate all previous poles and VGPs from the Río de la Plata Craton between around 600 and 575 Ma. These are mainly based on the well-dated poles of Playa Hermosa Formation (PH, ca. 594 Ma) and Sierra de las Animas Complex (ca. 578 Ma) plus the Los Barrientos (LB) pole, with a less well constrained age, but likely around 580 to 585 Ma from stratigraphic considerations as it belongs to the Cerro Largo Formation (see Gómez-Peral et al., 2018). Assuming an assembled West Gondwana, this fast section of the Rio de la Plata craton APWP is supported by the position of the Nola dykes pole (ND, ca. 571 Ma) from the Congo- São Francisco craton and the Adrar-*n*-Takoucht volcanics pole (C, ca. 577 Ma) from West Africa. A few VGPs from the Sierras Bayas Group (Rapalini et al., 2013, 2021) consistently fall along this path.

The positions of the Avellaneda (AV) and Cerro Negro (CN) Formations poles obtained in our study suggest that the Late Ediacaran path for the Rio de la Plata (and West Gondwana?) should be modified. The Avellaneda Formation paleomagnetic pole has a more likely age, limited by stratigraphic constraints, between 580 and 560 Ma. A negative C^{13} anomaly in its upper levels (e.g. Gómez-Peral et al., 2018, Afonso et al, 2022 companion paper) may be correlative of the Shuram global isotopic excursion, dated at 570 Ma (Gong and Li, 2020; Ronney et al., 2020). An age of 570 Ma or younger for the AV pole is also suggested for its position nearly 60° apart from the SAn, LB, ND and C poles of ca. 585–575 Ma. In any case, this implies a fast polar drift of CRP in the early Late Ediacaran and a path that turns into northern central Africa, different from most previously proposed Gondwana paths (Trindade et al., 2006; Rapalini et al., 2013). The less robust paleomagnetic pole obtained for the Cerro Negro Formation falls very close to AV pole. The age of this formation is restricted from the discoidal structures reported by Arrouy et al. (2016) in its upper levels. These structures were assigned to the genus *Aspidella* sp. and have been interpreted as corresponding to the "White Sea" fauna (Arrouy et al., 2016) for which a more likely age of 558–550 Ma has been proposed (Boag et al., 2016; Cracknell et al., 2021). CN pole was obtained from the lower levels of the Cerro Negro Formation. These considerations suggest that AV and CN poles are most likely encompassed in the 570–550 Ma. Of course, this is based on the acceptance of a primary magnetization for both units. Marginally positive tilt tests, rock magnetic data plus a coherent magnetostratigraphic pattern as shown in Fig. 19 and described in the companion paper (Afonso et al., 2022) are consistent with a primary remanence.

Robert et al. (2017) conducted paleomagnetic studies on well-dated volcanics in the West African craton. The authors proposed the existence of two events of inertial interchange true polar wander (IITPW) occurring in the Ediacaran. In particular, the second proposed event occurred

between 575 and 565 Ma and would explain the very distant paleomagnetic poles of the Adrar-*n*-Takoucht and Fajjoud and Taddoughast volcanics (Robert et al., 2017) of approximately those ages, respectively. Robert et al. (2018) further developed this model comparing approximately coeval paleomagnetic poles from West Africa, Laurentia, Baltica, West Gondwana and Australia that were interpreted to be compatible with the IITPW hypothesis. Ediacaran poles from West Africa (AD, B1, B2 and C, see Table 6, Fig. 20) show a long and fast track as well as an abrupt change in its direction determined by pole C of ~ 577 Ma. This pole is approximately consistent with poles of similar ages in RPC (SAn and LB) and Congo-São Francisco (ND), suggesting that these blocks were close to each other or even already united at that time. The AV and CN poles imply a fast apparent polar displacement for the RPC (and other West Gondwana blocks?) between ca. 580 and 570–550 Ma (Fig. 20). This seems consistent at a first sight with the IITPW proposal, although the RPC track falls short of a ca. 90º swath apparently found in other continents (Robert et al., 2018). Whether this is invalidating such model or just the recording of superposed independent tectonic movements along the TPW track during final Gondwana assembly should be investigated further. The role of long-lived large non-dipole contributions in the Late Ediacaran Earth magnetic field remain ambiguous. Consistent paleopole positions from different continents at around 580–575 Ma, as already discussed, suggest that the GAD hypothesis was likely valid at least near the end of the Early Ediacaran.

With the new paleomagnetic information for RPC, and assuming a basically valid GAD hypothesis up to ca. 550 Ma it is possible to infer a gross picture of the drift of this block during the late Early and early Late Ediacaran (Fig. 21). At ~ 600 Ma the craton might have been at a paleo latitude of ~ 19° S (as computed for the Olavarría city in the Tandilia System), according to the paleomagnetic pole from the Playa Hermosa Formation (Rapalini et al., 2015). Relative location of other Western Gondwana blocks are not well constrained paleomagnetically, particularly Congo- São Francisco lacks any paleomagnetic pole of similar age. Slightly older poles from West Africa and Amazonia (see Table 6) at 610–615 Ma, suggest that both blocks were probably a single plate relatively far-away from RPC. By ~ 580 Ma (Fig. 21), the RPC, Congo-São Francisco and West Africa cratons are reconstructed as already assembled, although minor relative movements among them are allowed from the data. They are the already mentioned SAn, LB, ND and C poles (Table 6). Although there is no paleomagnetic information on the Amazonia craton for this time, it is indirectly inferred that it was part of the same continent together with the RPC given the paleoreconstructions that locate Amazonia attached to West Africa since the Paleoproterozoic (see D'Agrella Filho et al., 2016 and references therein) and the consistent early Ediacaran poles already mentioned. In this context, the existence of the Clymene Ocean (Trindade et al., 2006) is in doubt from the paleomagnetic point of view. However, it is possible to continue supporting its existence by appealing to the uncertainty of the paleomagnetic method as suggested by Rapalini et al (2021), but maintaining that Clymene was a smaller ocean/sea. Some authors (Warren et al., 2014; Arrouy et al., 2016; Gómez-Peral et al., 2019; Arrouy and Gómez-Peral, 2021; among others) interpreted sedimentological, petrographic and geochemical evidence as consistent with the existence of Clymene, at least as a epeiric sea. By ~ 580 Ma, the Olavarría locality in the RPC was situated at ~ 46° S, drifting about 27° in 20 Ma. The Western Gondwana forming blocks may have drifted afterwards towards even higher latitudinal positions within a large counterclockwise rotation (Fig. 21). Deposition of the marls and shales of the Avellaneda Formation took place at those times at latitude of ~ 50°S. The CN pole suggests similar paleolatitudes around 560–550 Ma.

8. Conclusions

Detailed paleomagnetic studies were conducted in the Avellaneda (~570 Ma) and Cerro Negro (~555 Ma) Formations. In the former unit, sampling was carried out at an outcrop and in samples extracted from three different drill cores. In the second, the sampling was carried out in only one drill core. In both cases, new paleomagnetic poles were obtained: (AV, 1.0° S, 313.4° E, A_{95}: 5.9°) for the Avellaneda Formation and (CNc, 3.6° S, 307.8°E, A_{95}: 16.6°) for the Cerro Negro Formation. Rock magnetism analyses suggest that both magnetite and hematite, in variable proportion, carry the remanence. The new poles allow a more robust APWP for the RPC in the 600–550 Ma interval. A drift of the RPC from low latitude positions at 600 Ma (~19°S for the Olavarría city) towards positions of moderately high paleolatitudes (around 50° S) for the interval 580–550 Ma. A long APWP between around 580 and 570 Ma for the RPC mainly involved a very large counterclockwise rotation with minor paleolatitudinal change. Whether this movement can be associated, and therefore supports, proposals of IITPW during the transition between the Early and Late Ediacaran awaits more in depth analyses and further paleomagnetic data of such age from different Western Gondwana forming blocks.

CRediT authorship contribution statement

P.R. Franceschinis: Conceptualization, Methodology, Formal analysis, Investigation, Data curation, Writing – original draft, Visualization. **J.W. Afonso:** Conceptualization, Methodology, Formal analysis, Investigation, Data curation, Writing – review & editing. **M.J. Arrouy:** Conceptualization, Methodology, Validation, Formal analysis, Resources, Writing – review & editing. **L.E. Gómez-Peral:** Conceptualization, Methodology, Validation, Formal analysis, Resources, Writing – review & editing. **D. Poiré:** Conceptualization, Methodology, Validation, Formal analysis, Resources, Writing – review & editing. **R.I.F. Trindade:** Conceptualization, Methodology, Formal analysis, Resources, Writing – review & editing, Supervision, Funding acquisition. **A.E. Rapalini:** Conceptualization, Methodology, Formal analysis, Resources, Writing – review & editing, Supervision, Funding acquisition.

Declaration of Competing Interest

The authors declare that they have no known competing financial interests or personal relationships that could have appeared to influence the work reported in this paper.

Data availability

Data will be made available on request.

Acknowledgments

This study was supported by the CONICET (Argentina)-FAPESP (Brazil) 2016 agreement and the CONICET (Subsidio Unidad Ejecutora-IGEBA 2016) grant and FAPESP Thematic Project 2016/06114-6. Universidad de Buenos Aires (Grant 20020170100290BA) and ANPCyT (PICT 2018-01330) gave additional financial support. GMAP software by Torsvik (NGU) and Anisoft and Remasoft programs (AGICO, Inc.) were used to analyse the data. Matias Naselli and Fernando Almaraz kindly collaborated during preparation of samples and running of thermomagnetic and hysteresis curves. A special thanks to Cementos Avellaneda S.A. for facilitating access to the Cabañita quarry for field work and the study of the drill cores. Thorough and constructive reviews by Phil McCausland and Zheng Gong and suggestions by Editors A.E. S. Pisarevsky and W. Teixeira are kindly acknowledged.

Appendix 1

(See Fig. A1).

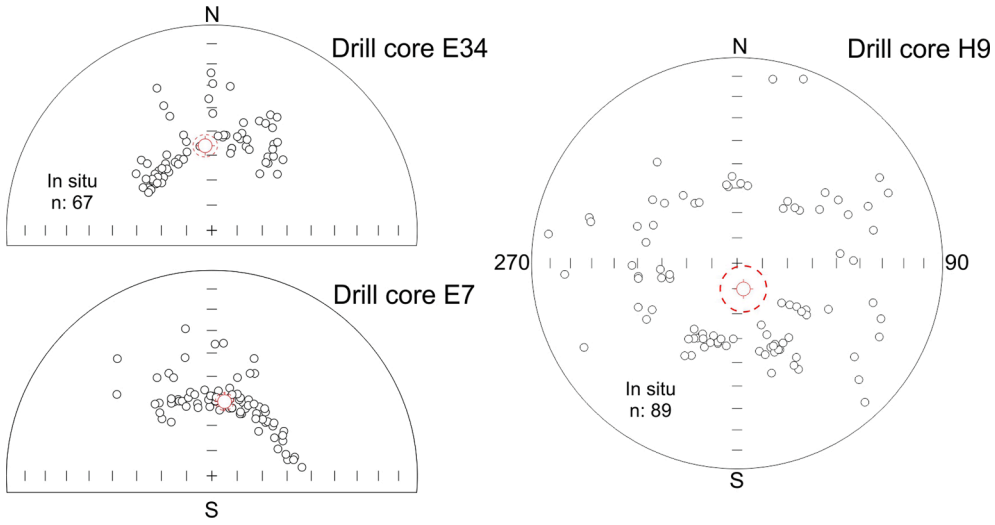

Fig. A1. Stereographic projections of the specimen directions obtained from the low coercivity component "A" for drill cores E34, H9 and E7. The directions are shown before azimuthal correction.

References

Abrajevitch, A., Van der Voo, R., 2010. Incompatible Ediacaran paleomagnetic directions suggest an equatorial geomagnetic dipole hypothesis. Earth Planet. Sci. Lett. 293, 164–170.

Ader, M., Macouin, M., Trindade, R.I.F., Hadrien, M., Yang, Z.Y., Sun, Z.M., Besse, J., 2009. A multilayered water column in the Ediacaran Yangtze platform? Insights from carbonate and organic matter paired δ13C. Earth Planet. Sci. Lett. 288, 213–227.

Ader, M., Sansjofre, P., Halverson, G.P., Busigny, V., Trindade, R.I., Kunzmann, M., Nogueira, A.C., 2014. Ocean redox structure across the Late Neoproterozoic Oxygenation Event: a nitrogen isotope perspective. Earth Planet. Sci. Lett. 396, 1–13.

Afonso, J. W. L., Franceschinis, P.R., Rapalini, A. E., Arrouy, M. J., Gómez-Peral., L., Poiré, D., Caetano-Filho, S., Trindade, R. I. F., 2022. Paleomagnetism of the Ediacaran Avellaneda Formation (Argentina), Part II: Magnetic and chemical stratigraphy constraints on the onset of the Shuram carbon excursion. Precambrian Research, submitted.

Arrouy, M.J., Gómez-Peral, L.E., 2021. Exposing the inside of the fine-grained siliciclastic tidal shelf deposits of the Alicia Formation, Tandilia Basin, during the Ediacaran anoxia in the Clymene Ocean. J. S. Am. Earth Sci. 102945.

Arrouy, M.J., Poiré, D., Gómez-Peral, L.E., Canalicchio, J.M., 2015. Sedimentología y estratigrafía del grupo La Providencia (nom. nov.): cubierta superior neoproterozoica, Sistema de Tandilia, Argentina. Latin American Journal of Sedimentology and Basin Analysis 22, 171–189.

Arrouy, M.J., Warren, L.V., Quaglio, F., Poiré, D.G., Simões, M.G., Rosa, M.B., Gómez-Peral, L.E., 2016. Ediacaran discs from South America: Probable soft-bodied macrofossils unlock the paleogeography of the Clymene Ocean. Sci. Rep. 6, 1–10.

Arrouy, M.J., Gaucher, C., Poiré, D.G., Xiao, S., Gómez-Peral, L.E., Warren, L.V., Bykova, N., Quaglio, F., 2019. A new record of late Ediacaran acritarchs from La Providencia group (Tandilia System, Argentina) and its biostratigraphical significance. J. S. Am. Earth Sci. 93, 283–293.

Arrouy, M.J., Gómez-Peral, L.E., Penzo, V., Ferreyra, C., Poiré, D.G., 2021. Fossil bubble structure related to microbial activity coeval with the middle Ediacaran Oceanic Oxygenation Event in the Tandilia System. Special Volume of Latin American Journal of Sedimentology and Basin Analysis 28, 101–120.

Boag, T.H., Darroch, S.A., Laflamme, M., 2016. Ediacaran distributions in space and time: testing assemblage concepts of earliest macroscopic body fossils. Paleobiology 42, 574–594.

Bono, R.K., Tarduno, J.A., Nimmo, F., Cottrell, R.D., 2019. Young inner core inferred from Ediacaran ultra-low geomagnetic field intensity. Nat. Geosci. 12, 143–147.

Borrello, A.V., 1966. Trazas, restos tubiformes y cuerpos fósiles problemáticos de la Formación La Tinta, Sierras Septentrionales de la Provincia de Buenos Aires. Paleontografía Bonaerense, Fasc. 5, Comisión de Investigaciones Científicas, Provincia de Buenos Aires 1-42.

Canfield, D.E., Poulton, S.W., Knoll, A.H., Narbonne, G.M., Ross, G., Goldberg, T., Strauss, H., 2008. Ferruginous conditions dominated later Neoproterozoic deep-water chemistry. Science 321, 949–952.

Cingolani, C.A., Hartmann, L.A., Santos, J.O.S., McNaughton, N.J., 2002. U-Pb SHRIMP dating of zircons from the Buenos Aires complex of the Tandilia belt, Río de La Plata craton, Argentina. Proc 15 Congreso Geológico Argentino (El Calafate, Santa Cruz). Actas 1, 149–154.

Collins, A.S., Pisarevsky, S.A., 2005. Amalgamating eastern Gondwana: the evolution of the Circum-Indian Orogens. Earth Sci. Rev. 71, 229–270.

Cordani, U.G., Pimentel, M.M., de Araújo, C.E.G., Fuck, R.A., 2013. The significance of the Transbrasiliano-Kandi tectonic corridor for the amalgamation of West Gondwana. Braz. J. Geol. 43, 583–597.

Cracknell, K., García-Bellido, D.C., Gehling, J.G., Ankor, M.J., Darroch, S.A., Rahman, I. A., 2021. Pentaradial eukaryote suggests expansion of suspension feeding in White Sea-aged Ediacaran communities. Sci. Rep. 11, 1–9.

D'Agrella Filho, M.S., Pacca, I.G., 1988. Palaeomagnetism of the Itajai, Castro and Bom Jardim groups from southern Brazil. Geophys. J. Int. 2, 365–376.

D'Agrella Filho, M.S., Trindade, R.I.F., Queiroz, M.V.B., Meira, V.T., Janikian, L., Ruiz, A. S., Bispo-Santos, F., 2016. Reassessment of Aguapeí (Salto do Céu) paleomagnetic pole, Amazonian Craton and implications for Proterozoic supercontinents. Precambr. Res. 272, 1–17.

Driscoll, P.E., 2016. Simulating 2 Ga of geodynamo history. Geophys. Res. Lett. 43, 5680–5687.

Egli, R., Chen, A. P., Winklhofer, M., Kodama, K. P., Horng, C. S., 2010. Detection of noninteracting single domain particles using first-order reversal curve diagrams. Geochemistry, Geophysics, Geosystems, 11.

Erwin, D.H., Laflamme, M., Tweedt, S.M., Sperling, E.A., Pisani, D., Peterson, K.J., 2011. The Cambrian conundrum: early divergence and later ecological success in the early history of animals. Science 334, 1091–1097.

Evans, D.A.D., 2003. True polar wander and supercontinents. Tectonophysics 362, 303–320.

Franceschinis, P.R., Rapalini, A.E., Bettucci, L.S., Dopico, C.M., Milanese, F.N., 2019. Paleomagnetic confirmation of the "unorthodox" configuration of Atlantica between 2.1 and 2.0 Ga. Precambr. Res. 334, 105447.

García, M.S.R., Trindade, R.I.F., ÁDAgrella-Filho, M.S.D., Pinho, F.E.C., Paulo, S., 2013. Paleomagnetismo do complexo alcalino Planalto da Serra (Mato Grosso): Implicações para a Formação do Gondwana. Latinmag Letters, 3, 1–8.

Gómez-Peral, L.E., Poiré, D.G., Strauss, H., Zimmermann, U., 2007. Chemostratigraphy and diagenetic constraints on Neoproterozoic carbonate successions from the Sierras Bayas Group, Tandilia System, Argentina. Chem. Geol. 237, 127–146.

Gómez-Peral, L.E., Kaufman, A.J., Julia, M., Richiano, S., Sial, A.N., Poiré, D.G., Ferreira, V.P., 2018. Preglacial palaeoenvironmental evolution of the Ediacaran Loma Negra Formation, far southwestern Gondwana, Argentina. Precambr. Res. 315, 120–137.

Gómez-Peral, L.E., Arrouy, M.J., Poiré, D.G., Cavarozzi, C.E., 2019. Redox-sensitive element distribution in the Neoproterozoic Loma Negra Formation in Argentina, in the Clymene Ocean context. Precambr. Res. 332, 1–16.

Gong, Z., Li, M., 2020. Astrochronology of the Ediacaran Shuram carbon isotope excursion. Oman. Earth and Planetary Science Letters 547, 116462.

Hernández, M., Arrouy, M.J., Scivetti, N., Franzese, J.R., Canalicchio, J.M., Poiré, D.G., 2017. Tectonic evolution of the Neoproterozoic Tandilia sedimentary cover, Argentina: New evidence of contraction and extensional events in the southwest Gondwana margin. J. S. Am. Earth Sci. 79, 230–238.

Iñiguez, A.M., Zalba, P.E., 1974. Nuevo nivel de arcilitas en la zona de Cerro Negro, Partido de Olavarría, Provincia de Buenos Aires. Anales del LEMIT, Serie 2, 95–100.

Kirschvink, J., 1980. The least-squares line and plane and the analysis of paleomagnetic data. Geophys. J. R. Astron. Soc. 62, 699–718.

Kopp, R.E., Kirschvink, J.L., 2008. The identification and biogeochemical interpretation of fossil magnetotactic bacteria. Earth Sci. Rev. 86, 42–61.

Koymans, M.R., Langereis, C.G., Pastor-Galan, D., van Hinsbergen, D.J.J., 2016. Paleomagnetism.org: An online multi-platform open source environment for paleomagnetic data analysis. Comput. Geosci. 93, 127–137.

Li, Z., Cao, M., Loyd, S.J., Algeo, T.J., Zhao, H., Wang, X., Zhao, L., Chen, Z.Q., 2020. Transient and stepwise ocean oxygenation during the late Ediacaran Shuram Excursion: Insights from carbonate δ238U of northwestern Mexico. Precambr. Res. 344, 105741.

Li, Z.X., Evans, D.A., Halverson, G.P., 2013. Neoproterozoic glaciations in a revised global palaeogeography from the breakup of Rodinia to the assembly of Gondwanaland. Sed. Geol. 294, 219–232.
Lyons, T.W., Reinhard, C.T., Planavsky, N.J., 2014. The rise of oxygen in Earth's early ocean and atmosphere. Nature 506, 307–315.
Macdonald, F.A., Strauss, J.V., Sperling, E.A., Halverson, G.P., Narbonne, G.M., Johnston, D.T., Kunzmann, M., Schrag, D.P., Higgins, J.A., 2013. The stratigraphic relationship between the Shuram carbon isotope excursion, the oxygenation of Neoproterozoic oceans, and the first appearance of the Ediacara biota and bilaterian trace fossils in northwestern Canada. Chem. Geol. 362, 250–272.
Marchese, H.G., Di Paola, E., 1975. Reinterpretación estratigráfica de la Perforación Punta Mogotes N° 1, Provincia de Buenos Aires. Revista de la Asociación Geológica Argentina 30, 17–44.
McElhinny, M.W., 1964. Statistical significance of the fold test in palaeomagnetism. Geophys. J. Int. 8, 338–340.
McFadden, P.L., McElhinny, M.W., 1988. The combined analysis of remagnetization circles and direct observations in palaeomagnetism. Earth Planet. Sci. Lett. 87, 161–172.
McFadden, P.L., McElhinny, M.W., 1990. Classification of the reversal test in palaeomagnetism. Geophys. J. Int. 103, 725–729.
McFadden, P.L., Reid, A.B., 1982. Analysis of palaeomagnetic inclination data. Geophys. J. Int. 69, 307–319.
Meert, J.G., 2014. Strange attractors, spiritual interlopers and lonely wanderers: The search for pre-Pangean supercontinents. Geosciencie Frontiers 5, 155–166.
Meert, J.G., Van der Voo, R., 1996. Study of the Sinyai Dolerite, Kenya: Implications for Gondwana Assembly. J. Geol. 104, 131–142.
Mitchell, R.N., Kilian, T.M., Evans, D.A., 2012. Supercontinent cycles and the calculation of absolute palaeolongitude in deep time. Nature 482, 208–211.
Moloto-A-Kenguemba, G., Trindade, R.I.F., Monié, P., Nédélec, A., Siqueira, R., 2008. A late Neoproterozoic paleomagnetic pole for the Congo craton: Tectonic setting, paleomagnetism and geochronology of the Nola dike swarm (Central African Republic). Precambr. Res. 164, 214–226.
Morel, P., 1981. Palaeomagnetism of a Pan-African diorite: a Late Precambrian pole for western Africa. Geophys. J. R. Astron. Soc. 65, 493–503.
Moskowitz, B.M., Frankel, R.B., Bazylinski, D.A., 1993. Rock magnetic criteria for the detection of biogenic magnetite. Earth Planet. Sci. Lett. 120, 283–300.
Poiré, D., Gaucher, C., 2009. Lithostratigraphy. Neoproterozoic- Cambrian evolution of the Río de la Plata Palaeocontinent. En: Gaucher C., Sial, A.N., Halverson, G.P., Frimmel, H.E. (Eds), Neoproterozoic–Cambrian Tectonics, Global Change and Evolution: a focus on southwestern Gondwana. Developments in Precambrian Geology, 16, 87–101.
Poiré D.G., Gaucher, C., Germs, G., 2007. La superficie 'Barker' y su importancia regional, Neoproterozoico del Cratón del Río de La Plata. VI Jornadas Geológicas y Geofísicas Bonaerenses. Actas 36. Mar del Plata, Argentina.
Poiré, D.G., Peral, L.E.G., Arrouy, M.J., 2018. The Glaciations in South America. In: Siegesmund, S., Basei, M.A.S., Oyhantçabal, P., Oriolo, S. (Eds.), Geology of Southwest Gondwana, Regional Geology Reviews. Springer International Publishing, Cham, pp. 527–541.
Pu, J.P., Bowring, S.A., Ramezani, J., Myrow, P., Raub, T.D., Landing, E., Mills, A., Hodgin, E., Macdonald, F.A., 2016. Dodging snowballs: Geochronology of the Gaskiers glaciation and the first appearance of the Ediacaran biota. Geology 44, 955–958.
Rapalini, A.E., 2006. New late Proterozoic paleomagnetic pole for the Rio de la Plata craton: Implications for Gondwana. Precambr. Res. 147, 223–233.
Rapalini, A.E., Sánchez Bettucci, L., 2008. Widespread remagnetization of late Proterozoic sedimentary units of Uruguay and the apparent polar wander path for the Rio de La Plata craton. Geophys. J. Int. 174, 55–74.
Rapalini, A.E., Trindade, R.I.F., Poiré, D.G., 2013. The La Tinta pole revisited: Paleomagnetism of the Neoproterozoic Sierras Bayas Group (Argentina) and its implications for Gondwana and Rodinia. Precambr. Res. 224, 51–70.
Rapalini, A.E., Tohver, E., Bettucci, L.S., Lossada, A.C., Barcelona, H., Pérez, C., 2015. The late Neoproterozoic Sierra de las Ánimas Magmatic Complex and Playa Hermosa Formation, southern Uruguay, revisited: Paleogeographic implications of new paleomagnetic and precise geochronologic data. Precambr. Res. 259, 143–155.
Rapalini, A.E., Franceschinis, P.R., Bettucci, L.S., Arrouy, M.J., Poiré, D.G., 2021. The Precambrian drift history and paleogeography of Río de la Plata craton. In: Pesonen, L.J., Salminen, J., Sten-Åke, E., Evans, D., Veikkolainen, T. (Eds.), Ancient Supercontinents and the Paleogeography of Earth. Elsevier, pp. 243–261.
Rapalini, A.E., 2018. The Assembly of Western Gondwana: Reconstruction Based on Paleomagnetic Data. In: Siegesmund, S., Basei, M.A.S., Oyhantçabal, P., Oriolo, Sebastián (Eds.), Geology of Southwest Gondwana. Regional Geology Reviews, Springer International Publishing, Cham, 3-18.
Robert, B., Besse, J., Blein, O., Greff-Lefftz, M., Baudin, T., Lopes, F., Meslouh, S., Belbadaoui, M., 2017. Constraints on the Ediacaran inertial interchange true polar wander hypothesis: A new paleomagnetic study in Morocco (West African Craton). Precambr. Res. 295, 90–116.
Robert, B., Greff-Lefftz, M., Besse, J., 2018. True polar wander: A key indicator for plate configuration and mantle convection during the late Neoproterozoic. Geochem. Geophys. Geosyst. 19, 3478–3495.
Roberts, A.P., Florindo, F., Villa, G., Chang, L., Jovane, L., Bohaty, S.M., Larrasoaña, J.C., Heslop, D., Gerald, J.D.F., 2011. Magnetotactic bacterial abundance in pelagic marine environments is limited by organic carbon flux and availability of dissolved iron. Earth Planet. Sci. Lett. 310, 441–452.
Roberts, A.P., Heslop, D., Zhao, X., Pike, C.R., 2014. Understanding fine magnetic particle systems through use of first-order reversal curve diagrams. Rev. Geophys. 52, 557–602.
Rooney, A.D., Cantine, M.D., Bergmann, K.D., Gomez-Pérez, I., Al Baloushi, B., Boag, T. H., Busch, J.F., Sperling, E.A., Strauss, J.V., 2020. Calibrating the coevolution of Ediacaran life and environment. Proc. Natl. Acad. Sci. 117, 16824–16830.
Sahoo, S.K., Planavsky, N.J., Jiang, G., Kendall, B., Owens, J.D., Wang, X., Shi, X., Anbar, A.D., Yons, T.W.L., 2016. Oceanic oxygenation events in the anoxic Ediacaran ocean. Geobiology 14, 457–468.
Smith, E.F., Macdonald, F.A., Petach, T.A., Bold, U., Schrag, D.P., 2016. Integrated stratigraphic, geochemical, and paleontological late Ediacaran to early Cambrian records from southwestern Mongolia. Bulletin 128, 442–468.
Sperling, E.A., Wolock, C.J., Morgan, A.S., Gill, B.C., Kunzmann, M., Halverson, G.P., Macdonald, F.A., Knoll, A.H., Johnston, D.T., 2015. Statistical analysis of iron geochemical data suggests limited late Proterozoic oxygenation. Nature 523, 451–454.
Tauxe, L., 2005. Lectures in Paleomagnetism. Electronic version 341.
Teixeira, W., Iacumin, M., Piccirillo, E.M., Echeveste, H., Ribot, A., Fernandez, R., Renne, P.R., Heaman, L.M., 2002. Calc-alkaline and tholeiitic dyke swarms of Tandilia, Rio de la Plata craton, Argentina: U-Pb, Sm-Nd and Rb-Sr 40Ar/39Ar data provide new clues for intraplate rifting shortly after the Trans-Amazonian orogeny. Precambr. Res. 119, 329–353.
Teixeira, W., D'Agrella Filho, M.S., Hamilton, M.A., Ernst, R.E., Girardi, V.A.V., Mazzucchelli, M., Bettencourt, J.S., 2013. U-Pb (ID-TIMS) baddeleyite ages and paleomagnetism of 1.79 and 1.59 Ga tholeiitic dyke swarms, and position of the Rio de la Plata Craton within the Columbia supercontinent. Lithos 174, 157–174.
Thallner, D., Biggin, A.J., Halls, H.C., 2021. An extended period of extremely weak geomagnetic field suggested by palaeointensities from the Ediacaran Grenville dykes (SE Canada). Earth Planet. Sci. Lett. 568, 117025.
Tohver, E., DAgrella-Filho, M.S.D., Trindade, R.I.F., 2006. Paleomagnetic record of Africa and South America for the 1200–500 Ma interval, and evaluation of Rodinia and Gondwana assemblies. Precambrian Research, 147, 193–222.
Tohver, E., Trindade, R.I., 2014. Comment on "Was there an Ediacaran Clymene Ocean in central South America?" by UG Cordani and others. Am. J. Sci. 314, 805–813.
Torsvik, T.H., Van der Voo, R., Preeden, U., Mac Niocaill, C., Steinberger, B., Doubrovine, P.V., van Hinsbergen, D.J.J., Domeier, M., Gaina, C., Tohver, E., Meert, J.G., McCausland, P.J.A., Cocks, L.R.M., 2012. Phanerozoic Polar Wander, Palaeogeography and Dynamics. Earth-Science Review 114, 325–368.
Trindade, R.I.F., D'Agrella Filho, M.S., Epof, I., Brito-Neves, B.B., 2006. Paleomagnetism of Early Cambrian Itabaiana mafic dikes (NE Brazil) and the final assembly of Gondwana. Earth Planetary Science Letters 244, 361–377.
Valencio, D.A., Sinito, A.M., Vilas, J.F., 1980. Palaeomagnetism of Upper Precambrian rocks of the La Tinta Formation, Argentina. Geophys. J. R. Astron. Soc. 62, 563–575.
Warren, L.V., Quaglio, F., Riccomini, C., Simões, M.G., Poiré, D.G., Strikis, N.M., Anelli, L.E., Strikis, P.C., 2014. The puzzle assembled: Ediacaran guide fossil Cloudina reveals an old proto-Gondwana seaway. Geology 42, 391–394.
Xiao, S., Zhou, C., Liu, P., Wang, D., Yuan, X., 2014. Phosphatized Acanthomorphic Acritarchs and Related Microfossils from the Ediacaran Doushantuo Formation at Weng'an (South China) and their Implications for Biostratigraphic Correlation. J. Paleontol. 88, 1–67.
Yuan, W., Zhou, H., Yang, Z., Hein, J.R., Yang, Q., 2019. Magnetite magnetofossils record biogeochemical remanent magnetization in hydrogenetic ferromanganese crusts. Geology 48, 298–302.